



Impacts of elevated anthropogenic emissions on physicochemical characteristics of black-carbon-containing particles over the Tibetan Plateau

Jinbo Wang^{1,2}, Jiaping Wang^{1,2,3}, Yuxuan Zhang^{1,2,3,4}, Tengyu Liu^{1,2,3}, Xuguang Chi^{1,2,3}, Xin Huang^{1,2}, Dafeng Ge^{1,2}, Shiyi Lai^{1,2}, Caijun Zhu^{1,2}, Lei Wang^{1,2,3}, Qiaozhi Zha^{1,2,3}, Ximeng Qi^{1,2,3}, Wei Nie^{1,2,3}, Congbin Fu^{1,2,3}, and Aijun Ding^{1,2,3}

¹Joint International Research Laboratory of Atmospheric and Earth System Sciences, School of Atmospheric Sciences, Nanjing University, Nanjing, 210023, China

²Jiangsu Provincial Collaborative Innovation Center of Climate Change, Nanjing, 210023, China

³National Observation and Research Station for Atmospheric Processes and Environmental Change in Yangtze River Delta, Nanjing, 210023, China

⁴Key Laboratory of Atmospheric Environment and Extreme Meteorology, Institute of Atmospheric Physics, Chinese Academy of Sciences, Beijing, 100029, China

Correspondence: Jiaping Wang (wangjp@nju.edu.cn)

Received: 24 March 2024 – Discussion started: 8 April 2024

Revised: 19 June 2024 – Accepted: 19 July 2024 – Published: 2 October 2024

Abstract. Black carbon (BC) in the Tibetan Plateau (TP) region has distinct climate effects that strongly depend on its mixing state. The aging processes of BC in the TP are subject to emissions from various regions, resulting in considerable variability of its mixing state and physicochemical properties. However, the mechanism and magnitude of this effect are not yet clear. In this study, field observations on physicochemical properties of BC-containing particles (PM_{BC}) were conducted in the northeast (Xihai) and southeast (Lulang) regions of the TP to investigate the impacts of transported emissions from lower-altitude areas on BC characteristics in the TP. Large spatial discrepancies were found in the chemical composition of PM_{BC} . Both sites showed higher concentrations of PM_{BC} when they were affected by transported air masses outside the TP but with diverse chemical composition. Source apportionment for organic aerosol (OA) suggested that primary OA in the northeastern TP was attributed to hydrocarbon OA (HOA) from anthropogenic emissions, while it was dominated by biomass burning OA (BBOA) in the southeastern TP. Regarding secondary aerosol, a marked enhancement in nitrate fraction was observed on aged BC coating in Xihai when the air masses were brought by updrafts and easterly winds from lower-altitude areas. With the development of boundary layer, the enhanced turbulent mixing promoted the elevation of anthropogenic pollutants. In contrast to Xihai, the thickly coated BC in Lulang was mainly caused by elevation and transportation of biomass burning plumes from south Asia, showing a large contribution of secondary organic aerosol (SOA). The distinct transported emissions lead to substantial variations of both chemical composition and light absorption ability of BC across the TP. The thicker coating and higher mass absorption cross-section (MAC) of PM_{BC} in air masses elevated from lower-altitude regions reveal the promoted BC aging processes and their impacts on the mixing state and light absorption of BC in the TP. These findings emphasize the vulnerability of plateau regions to influences of elevated emissions, leading to significant changes in BC concentration, mixing states and light absorption across the TP, all of which need to be considered in the evaluation of BC radiative effects for the TP region.

1 Introduction

The Tibetan Plateau (TP) is the largest plateau of the world, covering approximately 2.5×10^6 km². Its average altitude exceeds 4000 m, and its glaciers cover an area of over 100 000 km² (Yao et al., 2012a). As the third pole, the TP plays a crucial role in the Asian monsoon systems, the hydrological cycle and the global climate (Duan and Wu, 2005; Wu et al., 2007, 2015). Pollutants affect the ecological environment of the TP and its surrounding region significantly. They result in increased air temperature (Gustafsson and Ramanathan, 2016), changes in cloud properties (Hua et al., 2020; Lai et al., 2024), glacier retreat (Kang et al., 2010, 2019; Xu et al., 2009; Yao et al., 2012b), anomalies in the hydrological cycle (Luo et al., 2020; Yang et al., 2014; Menon et al., 2002; Ramanathan et al., 2005) and the Asian monsoon (Meehl et al., 2008).

Black carbon (BC) is one of the most important aerosol species affecting climate, glaciers and hydrology in the TP (Kopacz et al., 2011; Xu et al., 2009; Yang et al., 2022) because of distinct climate effects (Bond et al., 2013). It is generated by the incomplete combustion of fossil fuels and biomass and is also known as refractory BC (rBC). BC influences the climate directly because it can absorb short-wave radiation (Zhu et al., 2017). The climate forcing of BC is highly dependent on its mixing state. BC can be coated with non-refractory aerosol like organics, nitrate (NO₃⁻) and sulfate (SO₄²⁻) through condensation or coagulation and turns from an externally mixed to an internally mixed structure. The rBC mass absorption cross-section (MAC) of BC-containing particles (PM_{BC}) can be affected by non-refractory components coated on BC (Cai et al., 2022; Cheng et al., 2016; Gao et al., 2021; Liu et al., 2017; Schnaiter et al., 2005; Wang et al., 2023) via the “lensing effect” (Lack and Cappa, 2010), causing the change in radiative properties of BC. The cloud microphysical properties may also be altered when PM_{BC} are coated with hydrophilic materials and activated into cloud condensation nuclei (CCN), which influences climate indirectly (Bond et al., 2013; Dusek et al., 2006; Henning et al., 2010).

Previous studies have shown that BC has a remarkable direct radiative effect in the TP (Zhao et al., 2017; Liu et al., 2021). The radiative effects of BC are not only influenced by its concentration but also by its mixing state. In recent years, there has been an increasing number of field measurements of BC in the TP. It is reported that BC concentration can still occasionally reach high levels in the TP under certain meteorological and synoptic conditions (Babu et al., 2011; Zhu et al., 2016; Zhao et al., 2017). Observations of BC mixing states demonstrated that BC is mainly internally mixed (Yuan et al., 2019), and the BC coating enhances the MAC of BC in the TP (Wang et al., 2017; Wang et al., 2018; Chen et al., 2019; Tan et al., 2021). BC can be transported

over long distances with wildfire plumes (Huang et al., 2023; Zheng et al., 2020). Some regions of the TP may be affected by biomass burning (BB) from lower-altitude areas (Cao et al., 2010; Zhang et al., 2015; Cong et al., 2015). External transport can raise BC concentration and affect its morphology and mixing state in the TP (Tan et al., 2021; Chen et al., 2023). However, research on how emissions from various sources affect the chemical composition of PM_{BC} in the TP is scarce. Therefore, we conducted field observations of the physicochemical characteristics of PM_{BC} at two typical sites in the TP. The objective of this study is to investigate the impacts of various pollutant emissions and the subsequent regional transport, particularly those from anthropogenic activities from low-altitude regions, on the mixing state and chemical composition of PM_{BC} in the TP.

2 Materials and methods

2.1 Site description

Field measurements were conducted at two observation stations in the TP (Fig. 1). The station in the northeast TP is located in Xihai (~ 3100 m a.s.l.; 36°56' N, 100°54' E). The station in the southeast TP is the Southeast Tibet Plateau Observation and Research Station for the Alpine Environment, located in Lulang (~ 3200 m a.s.l.; 29°46' N, 94°44' E). The field campaign was conducted from 2 April to 16 May 2021 in Lulang and from 3 to 23 June 2021 in Xihai. Both stations are typical high-altitude sites of mountainous areas (Fig. 1a) but potentially influenced by distinct emission sources. There are more wildfires around Lulang (Fig. 1a), but Xihai is close to the northwest region of China, which is largely affected by anthropogenic emissions (Fig. 1b).

2.2 Instrumentation

The Soot Particle Aerosol Mass Spectrometer (SP-AMS, Aerodyne Inc., USA) was used to measure rBC and non-refractory materials coated on rBC (NR-PM_{BC}) (Onasch et al., 2012). The tungsten vaporizer was removed, and the intracavity infrared laser vaporizer was reserved to exclusively measure PM_{BC}. After adjusting the SP-AMS to the laser-only configuration, only PM_{BC} could be volatilized via the absorbing laser. We collected V-mode data due to their high sensitivity (DeCarlo et al., 2006). The total flow rate through the inlet was maintained at ~ 3 L min⁻¹. A PM_{2.5} cyclone was used in the front of the inlet (URG Corp., USA), and only particles in the size range of 50–1000 nm could be focused by the lens of inlet system. The bounce effect of aerosol was eliminated because the tungsten vaporizer was removed, so the usual collection efficiency (CE) (Docherty et al., 2013; Drewnick et al., 2005) was not applicable. The overlap of the particle beam and laser beam determined the CE of the SP-AMS with a laser-only configuration (Willis et al., 2014).

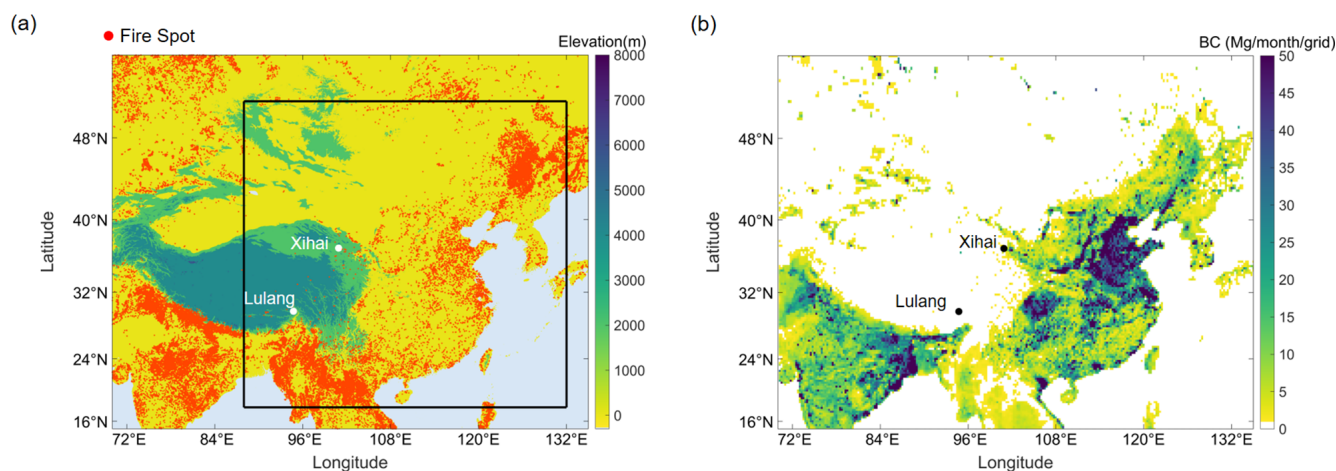


Figure 1. The maps showing (a) the topographic height and (b) the anthropogenic emissions of BC at the two measurement sites (Xihai, Lulang) and in the surrounding region. The red spots represent the fire spots during the field measurement period, and the square outlined in black represents the simulated domain.

The new CE was acquired by intercomparison of rBC concentration measured using the SP2 and SP-AMS (Massoli et al., 2015) and was nearly 1 during this campaign.

SP-AMS data were processed by standard time-of-flight AMS data analysis software packages (SQUIRREL version v1.60P and PIKA v1.20P). Ionization efficiency (IE) calibration was done shortly before removing the tungsten vaporizer. The mass-based calibration method was used to obtain IE values by sampling the 300 nm dried pure ammonium nitrate particles into the SP-AMS. The 300 nm particles were selected with a differential mobility analyzer (DMA, model 3081, TSI Inc., USA). The relative IE (RIE) for organic aerosol (OA) and SO_4^{2-} was 1.4 and 1.2, which was consistent with the RIE reported in a previous work (Canagaratna et al., 2007). The RIE for rBC was calibrated by sampling monodispersed 300 nm Regal Black particles in the SP-AMS. The detection limit was calculated based on the method in DeCarlo et al. (2006), and the detection limit of ammonium was higher, so the concentration of ammonium was estimated by ionic equilibrium. OA measured by the SP-AMS was subdivided into factors with different characteristics and sources based on positive matrix factorization (PMF) results (Zhang et al., 2005b, 2011). The PMF Evaluation Tool version 3.04A was used to perform PMF analysis on the high-resolution organic mass spectra (Ulbrich et al., 2009). Only ions with a mass-to-charge ratio below approximately 115 were considered in the PMF analysis.

The meteorological parameters, aerosol optical properties and gaseous pollutants were also measured simultaneously. Ozone (O_3), carbon monoxide (CO), nitric oxide (NO), nitrogen oxides (NO_x) and sulfur dioxide (SO_2) were measured using online analyzers (Teledyne API Inc., USA). The photoacoustic extinctions (PAX, Droplet Measurement Technologies Inc., USA) measured light absorption coefficients. Temperature, relative humidity (RH) and other meteorolog-

ical parameters were monitored by meteorological sensors (WXT530, Vaisala Inc., Finland).

2.3 Model configuration

In this study, we conducted regional chemical transport modeling using the Weather Research and Forecasting model coupled with Chemistry (WRF-Chem, version 3.7.1). This model encompasses a broad spectrum of physical and chemical processes, addressing the emission and deposition of pollutants, advection, diffusion, and gaseous and aqueous chemical transformations, as well as aerosol chemistry and dynamics (Grell et al., 2005). The model domain was centered at 35°N , 110°E with a grid resolution of 20 km, covering the northeastern Tibetan Plateau. The vertical structure of the model comprised 30 layers extending from the surface to the top pressure of 50 hPa. The simulation was conducted for a longer period including the time of the whole campaign from 3 to 23 June 2021. To establish accurate initial and boundary conditions for meteorological fields, we updated the model using 6-hourly $1^\circ \times 1^\circ$ National Centers for Environmental Prediction (NCEP) FNL (final) global analysis data. In our pursuit of capturing the meteorological fields well, we assimilated NCEP Automated Data Processing (ADP) operation global surface observation and global upper-air observational weather data. This assimilation process utilized default nudging coefficients for wind, temperature, and moisture.

The Yonsei University planetary boundary layer (YSU PBL) scheme was used to parameterize boundary layer processes (Hong et al., 2006). Other essential physical parameterization options included the unified Noah land surface model (Ek et al., 2003), the Lin microphysics scheme (Lin et al., 1983) and the Grell–Freitas cumulus parameterization scheme (Grell and Freitas, 2014). For representing atmo-

spheric chemistry numerically, we utilized the Carbon Bond Mechanism version Z photochemical mechanism along with the Model for Simulating Aerosol Interactions and Chemistry aerosol module (MOSAIC; Zaveri and Peters, 1999; Zaveri et al., 2008). Both natural and anthropogenic emissions were considered in this regional WRF-Chem modeling study. Anthropogenic emissions were derived from the Multi-resolution Emission Inventory for China (MEIC, 2023), which includes emissions from power plants, residential combustion, industrial processes, on-road mobile sources and agricultural activities (Li et al., 2017a). Biogenic emissions were calculated online using the Model of Emissions of Gases and Aerosols from Nature (MEGAN), encompassing more than 20 biogenic species (Guenther et al., 2006).

A comprehensive overview of the model configuration can be referenced in earlier investigations (Huang et al., 2016; Huang et al., 2018). Additionally, key configurations and validation for the WRF-Chem regional modeling are shown in Table S1 and Fig. S1 in the Supplement.

2.4 Other materials

The transport and emission conditions were considered in order to investigate their impacts on BC physical and chemical properties. The Hybrid Single-Particle Lagrangian Integrated Trajectory (HYSPLIT) model was used to calculate and cluster 72 h backward trajectories (Stein et al., 2015; Xu et al., 2018). The starting points of the simulation were Xihai and Lulang, and particles were released at a height of 1000 m above the ground level. The backward trajectories were calculated every hour during the field campaign. The boundary layer height is from the ECMWF Reanalysis v5 (Hersbach et al., 2023). The Fire Inventory from NCAR (FINN) was adopted to estimate daily open BB emissions with high spatial resolution (1 km) during the campaign (Wiedinmyer et al., 2006, 2011, 2022, 2023), and the anthropogenic emissions of major pollutants (MIX, 2021) were estimated using the MIX-Asia emission inventory (Li et al., 2017b).

Further, the optical properties of PM_{BC} were investigated based on the widely used core-shell Mie model (Bohren and Huffman, 1983; Virkkula, 2021). The MAC and the absorption enhancement (E_{abs}) of PM_{BC} were calculated following the algorithm developed by Mätzler (2002). The refractive index was $1.95-0.79i$ for rBC (Bond and Bergstrom, 2006) and $1.52-10^{-6}i$ for BC coating (Pitchford et al., 2007) at 550 nm wavelength. The calculated optical properties of PM_{BC} in PM_1 were validated with good agreement with observed results of BC in $\text{PM}_{2.5}$ (Fig. S2).

3 Results and discussion

3.1 Overview of BC properties and meteorological conditions in the TP

Figure 2 presents the overall conditions during the campaign. The mass concentration of rBC shows large temporal variation at both sites, with ranges of $0.02-1.28 \mu\text{g m}^{-3}$ in Xihai and $0.02-2.22 \mu\text{g m}^{-3}$ in Lulang. PM_{BC} concentration and light absorption coefficients (b_{abs}) increased in the latter period of Xihai campaign, contrasting with the marked decreasing pattern in PM_{BC} concentration and b_{abs} observed during the latter period of Lulang campaign. In Xihai, the concentration and proportion of inorganic components, especially NO_3^- , rose in the latter phase of the campaign as the wind direction (WD) shifted to a southeasterly one (Fig. 2f). The RH also got higher with the change of wind direction. Another major feature is that the wind direction had distinct diurnal variations. In Xihai, the wind direction converted from easterly and northeasterly flows during the nocturnal hours to southerly direction during daytime. Conversely, Lulang is predominantly controlled by northerly to northeasterly winds throughout the campaign period. Nevertheless, the wind speed (WS) was similar in Xihai and Lulang, with mean values of 1.8 ± 1.2 and $1.5 \pm 1.2 \text{ m s}^{-1}$, respectively. In terms of gaseous pollutants, higher levels of NO_x and O_3 were observed in Xihai (5.3 ± 3.4 and 48 ± 13 ppb) than in Lulang (4.0 ± 2.5 and 35 ± 15 ppb).

We also compared the observed BC concentration at different sites of the TP. Note that the term “black carbon” (BC) has not been used rigorously or consistently throughout all the previous modeling and measurement literature (Bond et al., 2013). Similar terms including “rBC”, “equivalent BC (eBC)” and “elemental carbon (EC)” have also been widely used corresponding to different measurement techniques. BC measured by laser-induced techniques is often referred to as “rBC”, and measured BC using light absorption (e.g., Aethalometer, AE) and thermal-optical methods is normally named “eBC” and “EC”, respectively. In Table 1, BC concentrations in the TP measured by several common techniques were collected and grouped according to the methods to make clearer comparison. Compared to measurements using the same instrument in a metropolitan area (Cui et al., 2022), the rBC concentration of the TP ($0.24 \pm 0.20 \mu\text{g m}^{-3}$) was approximately 25 % of Shanghai ($0.92 \pm 0.81 \mu\text{g m}^{-3}$). The rBC concentration in Xihai was relatively high compared to the southeastern and central TP, measured using the same technique (Table 1). This was potentially attributed to the strong BC emissions in the surrounding area of the northeast TP (Fig. 1). The rBC concentration in Lulang exhibited a relatively lower mean value yet with a broad range of variation, suggesting that BC may be subject to diverse air masses with significant discrepancies in emission intensity across the southeast and southern regions of the TP (Fig. 1). Higher BC levels were observed at stations in proximity to

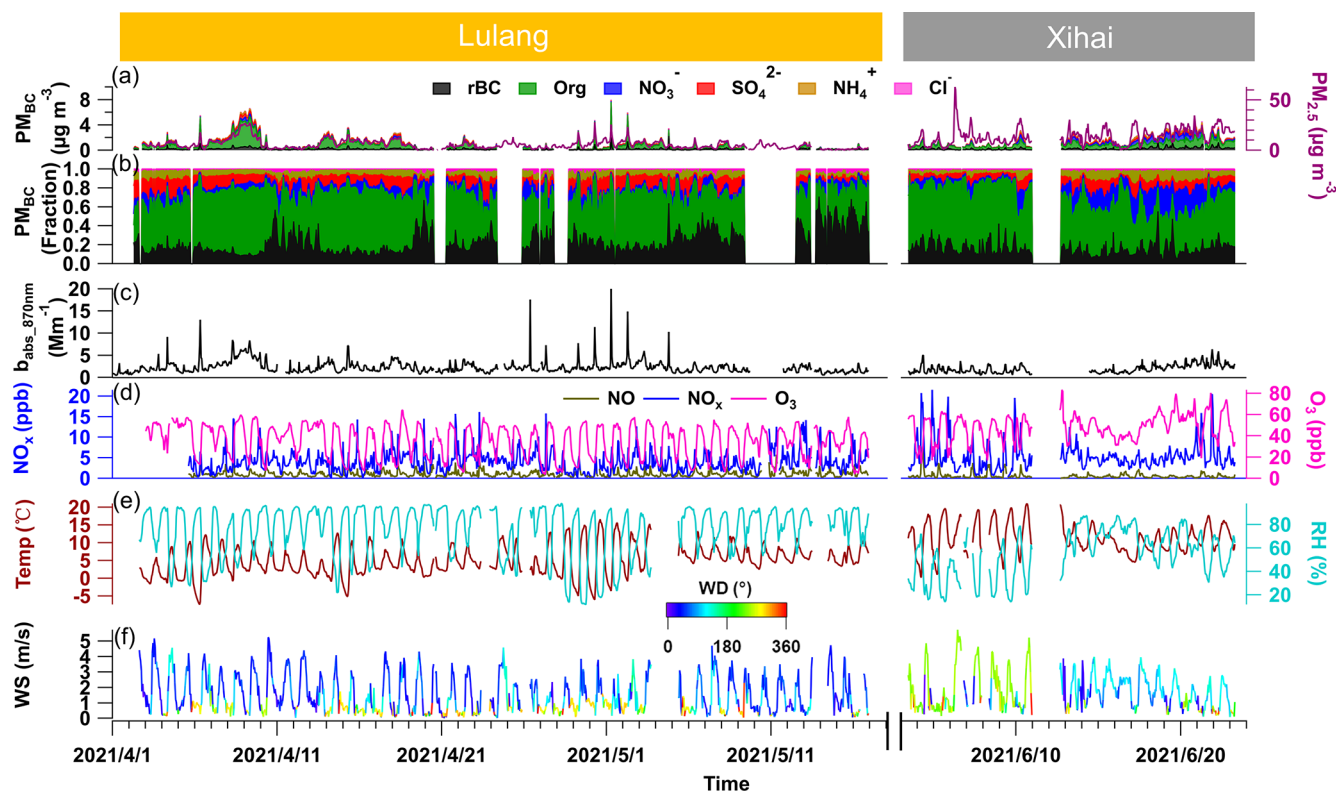


Figure 2. The time series of (a) mass concentrations of particulate matters (PM_{2.5}), refractory black carbon (rBC), organics (Org), nitrate (NO₃⁻), sulfate (SO₄²⁻), ammonium (NH₄⁺) and chloride (Cl⁻) in PM_{BC}; (b) mass fraction of different species in PM_{BC}; (c) aerosol light absorption coefficients (*b*_{abs}) at 870 nm wavelength; (d) gaseous pollutants including nitric oxide (NO), nitrogen oxide (NO₂) and ozone (O₃); (e) air temperature (Temp) and relative humidity (RH); and (f) wind direction (WD) and wind speed (WS).

Mainland Southeast Asia and the wider area of south Asia, where wildfire activities were extremely intense in spring. Therefore, the considerable variability of rBC concentrations in Lulang is likely due to the alternating influences from air masses transporting BB plumes and those originating from cleaner environments.

3.2 Physicochemical characteristics of BC-containing particles in the TP

The overall characteristics of PM_{BC} in Xihai and Lulang were compared based on statistical results. As Fig. 3a and b show, the mass concentration of rBC and PM_{BC} were higher in Xihai due to possible impacts of stronger anthropogenic emissions (Fig. 1b), and the difference ($t_{\text{rBC}} = 2.8$, $t_{\text{PM}_{\text{BC}}} = 2.1$) between the two sites was shown by the *t* test ($\alpha = 0.05$, $\nu = 50$). Figure 3c compares the mixing state of PM_{BC} in Xihai and Lulang, which was expressed by the mass ratio of BC coating to rBC (R_{BC}). The frequency distribution of R_{BC} showed an obvious difference at the two sites. R_{BC} in Xihai was generally higher than in Lulang, indicating the thicker coating in Xihai. The peak of R_{BC} occurred at [4.5,6] and [1.5,3] in Xihai and Lulang, respectively. R_{BC} of more than 50 % PM_{BC} was between 3.0 and

7.5, and only 11 % PM_{BC} had R_{BC} less than 3.0 in Xihai. Unlike Xihai, the percentage of thinly coated PM_{BC} for which R_{BC} was less than 3.0 was higher in Lulang at 33 %. The difference in mixing states of PM_{BC} was also demonstrated by the *t* test ($t_{R_{\text{BC}}} = 2.4$). The peak of MAC at both sites was between 12 and 14 m² g⁻¹ (Fig. 3d) which was significantly greater than the MAC of BC without coating (Bond and Bergstrom, 2006), and the average value and range of MAC in Xihai and Lulang were 12.8 (5.6–17.4) and 12.3 (6.8–15.7) m² g⁻¹. Over 61 % of BC was distributed in the larger MAC range (higher than 12.5 m² g⁻¹) in Xihai, showing stronger light absorption ability of BC in this region. Due to the synergy of higher mass concentration and light absorption ability, PM_{BC} could have larger climate effects in the northeast TP.

The chemical characteristics and sources of OA in PM_{BC} were identified by PMF. OA was separated into primary OA (POA) and oxygenated OA (OOA) at both sites (Figs. 4 and S3). In Xihai, there was one factor originating from primary emissions, and there were two factors from secondary formation. The POA factor had a higher signal of C₄H₇⁺ and C₄H₉⁺, which are important alkyl fragments from primary sources (Hu et al., 2016), in its mass spectrum. It also

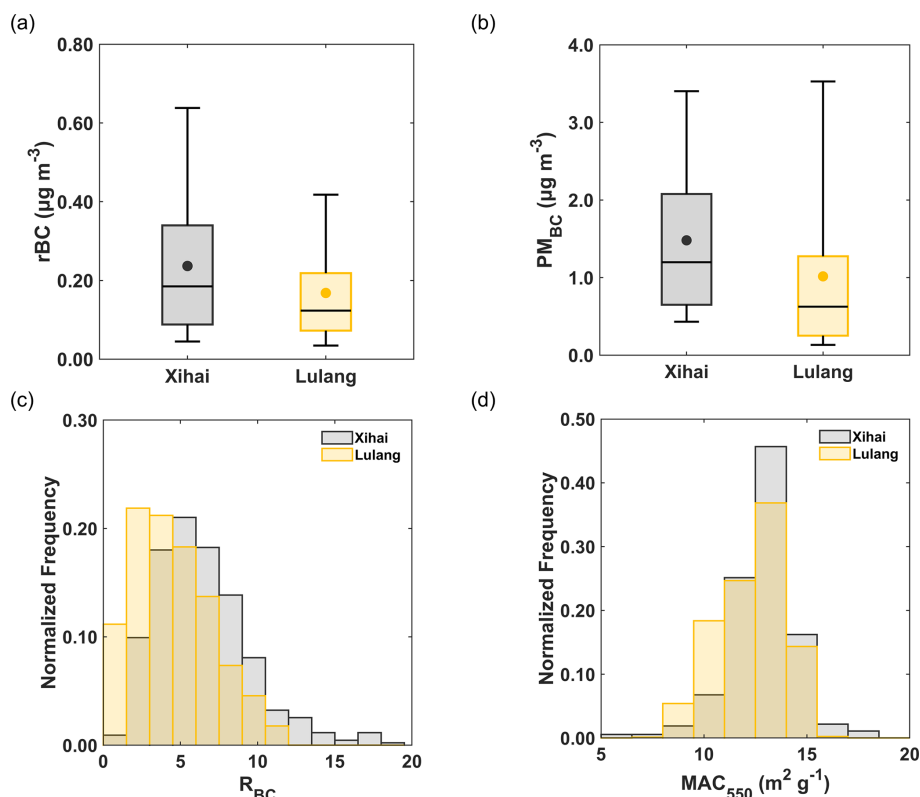


Figure 3. The box plots of (a) rBC and (b) BC-containing particles mass concentrations in Xihai and Lulang, where the lower and upper lines of the box plot represent the 25th and 75th percentiles and the whiskers stand for 5th and 95th values. The normalized frequency distribution charts show (c) the mass ratio of coating substance to the rBC core (R_{BC}) and (d) the mass absorption cross-section (MAC). Only 1.15 % of the R_{BC} exceeded the maximum value of the bin (19.5) in Xihai, and no R_{BC} exceeded the maximum value of the bin in Lulang.

had higher content of hydrogen; H : C was up to 1.84, and it had a lower signal of $\text{C}_2\text{H}_4\text{O}_2^+$, which is the typical BB tracer. Hence, this factor was mainly emitted from fossil fuel combustion rather than BB and was named hydrocarbon OA (HOA). OOA factors were further divided into less-oxidized OOA (LO-OOA) and more-oxidized OOA (MO-OOA) factors. These two factors constitute secondary OA (SOA) formed through oxidation processes such as photochemical reactions (Kanakidou et al., 2005; Zhang et al., 2005a; Zhao et al., 2018). They had a higher fraction of the signal of the CO_2^+ ion (m/z 44) and other oxygenic ions in the mass spectrum, which is similar to the mass spectra of typical OOA reported in other field campaigns (Crippa et al., 2013; Hu et al., 2016; Kim et al., 2020; Lee et al., 2017; Sun et al., 2016; Sun et al., 2020; Wang et al., 2016; Zhou et al., 2018). The O : C of the two OOA factors was also calculated (Canagaratna et al., 2015) to learn about the oxidation degree of OOA. MO-OOA exhibited a higher O : C ratio (0.84) than LO-OOA (0.49). Unlike Xihai, the POA factor in Lulang had a higher fraction of the signal of the $\text{C}_2\text{H}_4\text{O}_2^+$ (m/z 60) ion ($f_{\text{C}_2\text{H}_4\text{O}_2^+}$) in the mass spectrum, which is the fragment of levoglucosan mainly from BB (Lee et al., 2010). Therefore, this POA factor was identified as biomass burning OA

(BBOA) in Lulang. Moreover, the $f_{\text{CO}_2^+}$ and $f_{\text{C}_2\text{H}_4\text{O}_2^+}$ (0.065 versus 0.025) of this factor were also within the triangle area in a previous BBOA study (Cubison et al., 2011), and the $f_{\text{C}_2\text{H}_4\text{O}_2^+}$ was lower than the fresh BBOA, indicating that this factor was influenced by biomass burning activities and aging processes collectively. The remaining two factors were from SOA formation in Lulang and had a higher fraction of the signal of the CO_2^+ ion. Based on the oxidation degree, the two factors were identified as MO-OOA and LO-OOA. The O : C of MO-OOA and LO-OOA was 0.95 and 0.46, respectively. Compared to Lulang, the OA in BC coating was under stronger impacts of anthropogenic emissions in Xihai, indicated by HOA.

Figure 5 presents PM_{BC} chemical composition at two sites. BC coating had a higher mass contribution to PM_{BC} in Xihai and Lulang compared to the urban site (Collier et al., 2018), indicating the thick coating of PM_{BC} in the TP. The average mass fraction and concentration of BC coating were 84 % and $1.2 \mu\text{g m}^{-3}$ in Xihai. The mass fraction of coating was similar (83 %) in Lulang, although the concentration of BC coating was lower ($0.85 \mu\text{g m}^{-3}$). OA was the dominant component of BC coating (Fig. 5a) at both sites, which was consistent with the observation in the cen-

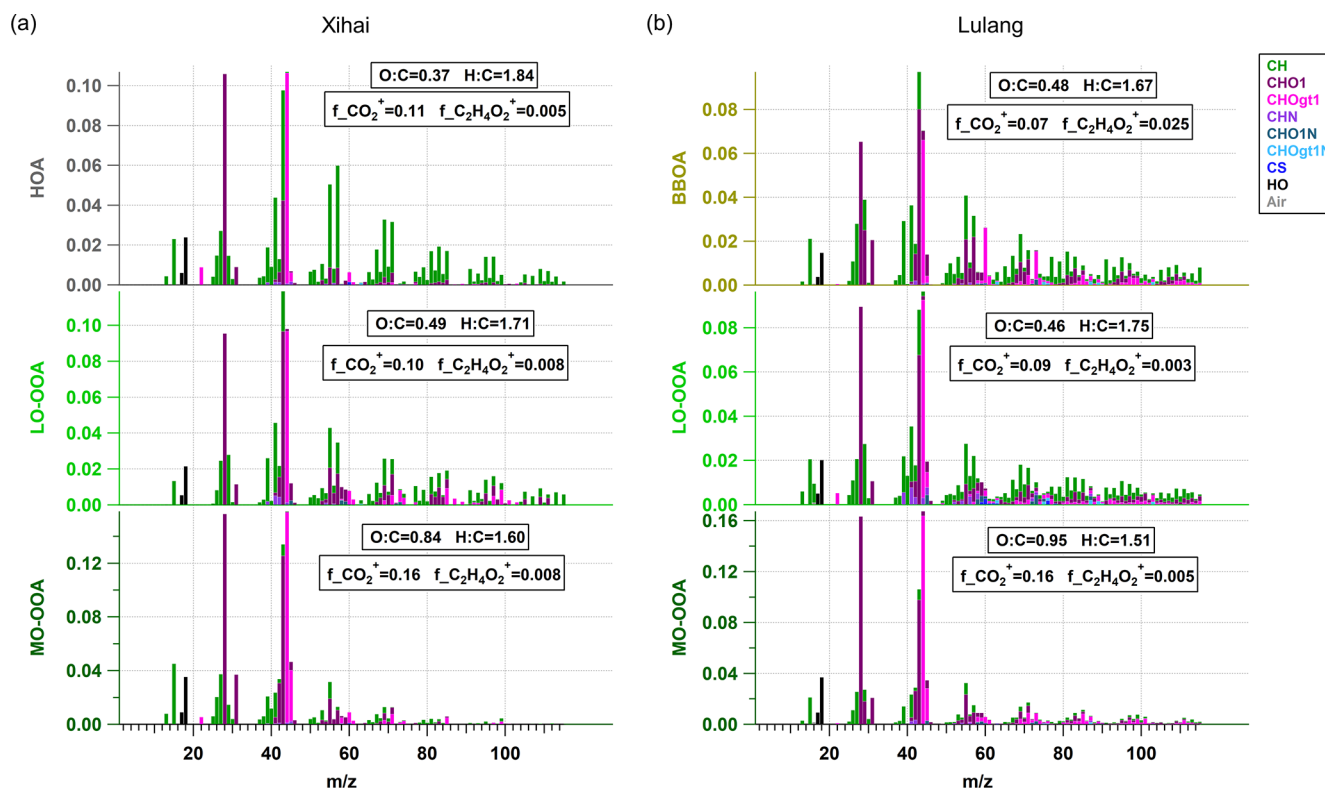


Figure 4. The mass spectra of different factors represents organic aerosol from specific sources in BC-containing particles in (a) Xihai and (b) Lulang. MO-OOA is more oxidized oxygenated organic aerosol, LO-OOA is less oxidized oxygenated organic aerosol, HOA is hydrocarbon-like organic aerosol and BBOA is biomass burning organic aerosol.

tral TP (Wang et al., 2017). OA took up a higher proportion of BC coating in Lulang compared to Xihai, Shanghai (Cui et al., 2022) and Fresno (Collier et al., 2018). During the field campaign, the average concentration of HOA, LO-OOA and MO-OOA was 0.25, 0.18 and 0.28 $\mu\text{g m}^{-3}$ in Xihai. MO-OOA also had the highest concentration (0.32 $\mu\text{g m}^{-3}$) of OA in Lulang and exceeded BBOA (0.15 $\mu\text{g m}^{-3}$) and LO-OOA concentration (0.14 $\mu\text{g m}^{-3}$). It demonstrated that SOA formation plays an important role in the coating process of PM_{BC} . The BC coating was dominated by MO-OOA, which was importantly affected by atmospheric oxidizing process. The concentration of O_3 highly relative to atmospheric oxidizing capacity improved significantly in the afternoon (Fig. S8), and the enhanced oxidizing capacity could cause an increase in MO-OOA in BC coating in both Xihai and Lulang. Besides MO-OOA, NO_3^- (17%) and HOA (35%) also made a large contribution to BC coating (Fig. 5a) and coated OA (Fig. 5b) in Xihai compared to Lulang. The HOA and NO_3^- were both closely associated with anthropogenic sources because the anthropogenic sources emitted HOA (Zhang et al., 2005a) and precursors of NO_3^- largely (Dall'Osto et al., 2009; Richter et al., 2005; Sun et al., 2018). This indicates that anthropogenic emissions have a strong influence on the coating process of PM_{BC} in the northeast TP, which is quite different from the southeast TP.

Figure 6 shows the coating components of BC with different R_{BC} in Xihai and Lulang. The mass fraction of MO-OOA was predominant in the thickly coated PM_{BC} in both Xihai and Lulang. Notably, a more significant enhancement in MO-OOA contribution within the thickly coated PM_{BC} was exhibited in Lulang, concomitant with a reduced fraction of inorganic components. The mass fraction of MO-OOA was only 9% in the thin BC coating ($R_{\text{BC}} < 1.5$), rising dramatically to 59% in those with R_{BC} exceeding 10.5 (thick BC coating). Another notable feature of the coating components was the higher contribution of BBOA in Lulang, especially when the coating thickness of PM_{BC} was higher. This indicates that thickly coating of BC was affected by BB activities and atmospheric oxidation significantly. In contrast to Lulang, HOA contribution decreased with the growth of R_{BC} , indicating a weaker effect of primary aerosol on thickly coated PM_{BC} in Xihai. Besides the MO-OOA, NO_3^- also contributed significantly to the composition of thickly coated PM_{BC} in Xihai, while the contribution of NO_3^- dropped with the rise of R_{BC} in Lulang. As illustrated in Fig. 6a, the mass fraction of NO_3^- reached 35% in the maximum bin of R_{BC} (18–19.5) in Xihai. The abundant NO_3^- was closely associated with anthropogenic sources, as mentioned in the preceding paragraph. The results demonstrate substantial variability in the composition influencing BC aging across the TP, af-

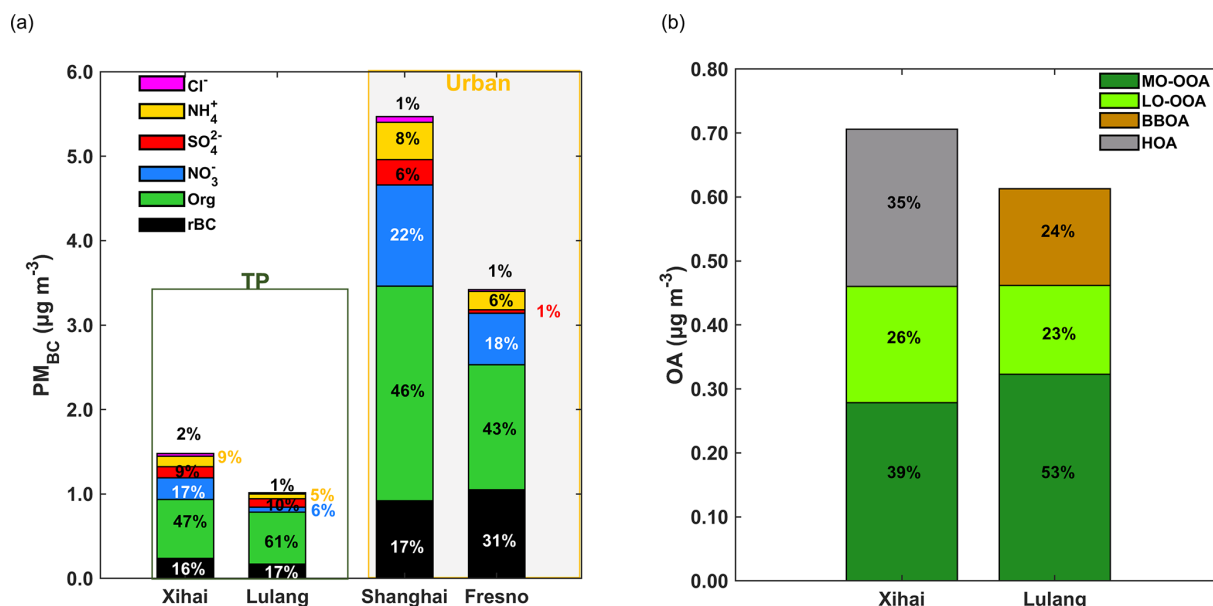


Figure 5. The stacked bars represent mass concentrations of (a) different species in BC-containing particles (PM_{BC}) and (b) different factors of organic aerosol in BC-containing particles. The numbers on the plot show the percentage of different species and organic factors. In panel (a), PM_{BC} in the TP (this study) was compared to PM_{BC} in urban regions (Collier et al., 2018; Cui et al., 2022).

affected by diverse emission sources. Moreover, anthropogenic pollutant emissions had strong impacts on BC coating, even in the remote highland areas, and the contribution of inorganic aerosol to BC coating is non-negligible in the TP.

3.3 Impacts of transported emissions on BC-containing particles

As discussed above, PM_{BC} in the TP region is possibly affected by both anthropogenic sources and BB transported from surrounding areas. To further investigate the impact mechanism of regional transport on BC, the cluster analysis of backward trajectories was carried out during field campaign of Xihai and Lulang, and backward trajectories were clustered into three kinds. In Xihai, the air masses were dominantly from the eastern region outside of the TP, as indicated by air masses of cluster1 (CL1), followed by the air masses of cluster2 (CL2) from the northwest of Xihai and the air masses of cluster3 (CL3) from the west of Xihai (Fig. 7a). PM_{BC} was brought more to Xihai (Fig. 7c) by the air masses of CL1, which went through the lower-altitude regions with stronger anthropogenic BC emissions (Figs. 7a and 1b). In Lulang, the CL1 air masses from south Asia were heavily polluted and aged; the CL2 air masses from southern edge of Himalayas and the CL3 air masses from central inland of the TP were cleaner (Fig. 7b). Comparing the polluted air masses (CL1) at two sites, the chemical composition of PM_{BC} showed an obvious difference between Xihai and Lulang (Fig. 7c and d). The contribution of inorganic species to BC coating was higher in Xihai, and there was more OA (especially MO-OOA) in polluted air mass of Lulang. MO-

OOA was the major component of BC coating in CL1 in Lulang. As shown by Fig. 7b, there were intensive wildfires in the source region of CL1 air masses of Lulang, and the wildfire plume could be readily uplifted to higher altitudes due to prevailing upflow driven by the lifting of the plume (Freitas et al., 2007; Fromm et al., 2000; Labonne et al., 2007; Luderer et al., 2006; Sofiev et al., 2012) or large-scale westerly and small-scale southerly circulations during the pre-monsoon season (Zhang et al., 2020; Cao et al., 2010). Such circulation could transport BC and other co-emitted pollutants from wildfires in Mainland Southeast Asia and the wider area of south Asia over the mountains of the TP until they reached Lulang. Because the biomass burning during wildfires can emit plentiful volatile organic compounds (VOCs) like terpenes (Akagi et al., 2013; Fiddler et al., 2024), it is expected that SOA can be formed through oxidation from precursors in the plume, leading to a thick coating on PM_{BC}. In Xihai, NO₃⁻ was one of the major coating species in PM_{BC} in CL1 (Fig. 7c) with mass concentration of NO₃⁻ of up to 0.35 µg m⁻³ (accounting for 19% of PM_{BC}), and other air mass clusters had a higher mass fraction of HOA in BC coating, indicating that PM_{BC} was less affected by oxidation and was fresher. CL1 transported air masses from the northwest region of China where the anthropogenic emissions are much stronger than the TP (Fig. 7a). With higher concentrations of primary pollutants like NO_x, the formation and coating of NO₃⁻ can be enhanced in PM_{BC}. The above results indicate that the effects of emission sources were discrepant in different regions of the TP, and the northeast part of the TP was significantly affected by anthropogenic emissions.

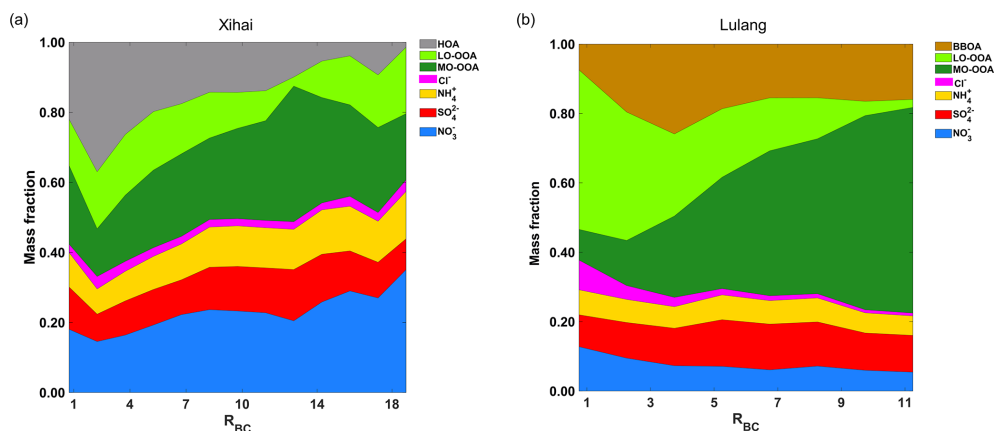


Figure 6. The variation of BC coating composition with R_{BC} between (a) Xihai and (b) Lulang. The x axis represents the mass ratio of BC coating components and rBC cores (R_{BC}), and the y axis represents the mass fractions of BC coating components coated on rBC. The mass fraction of components was averaged in each bin of R_{BC} (bin width: 1.5).

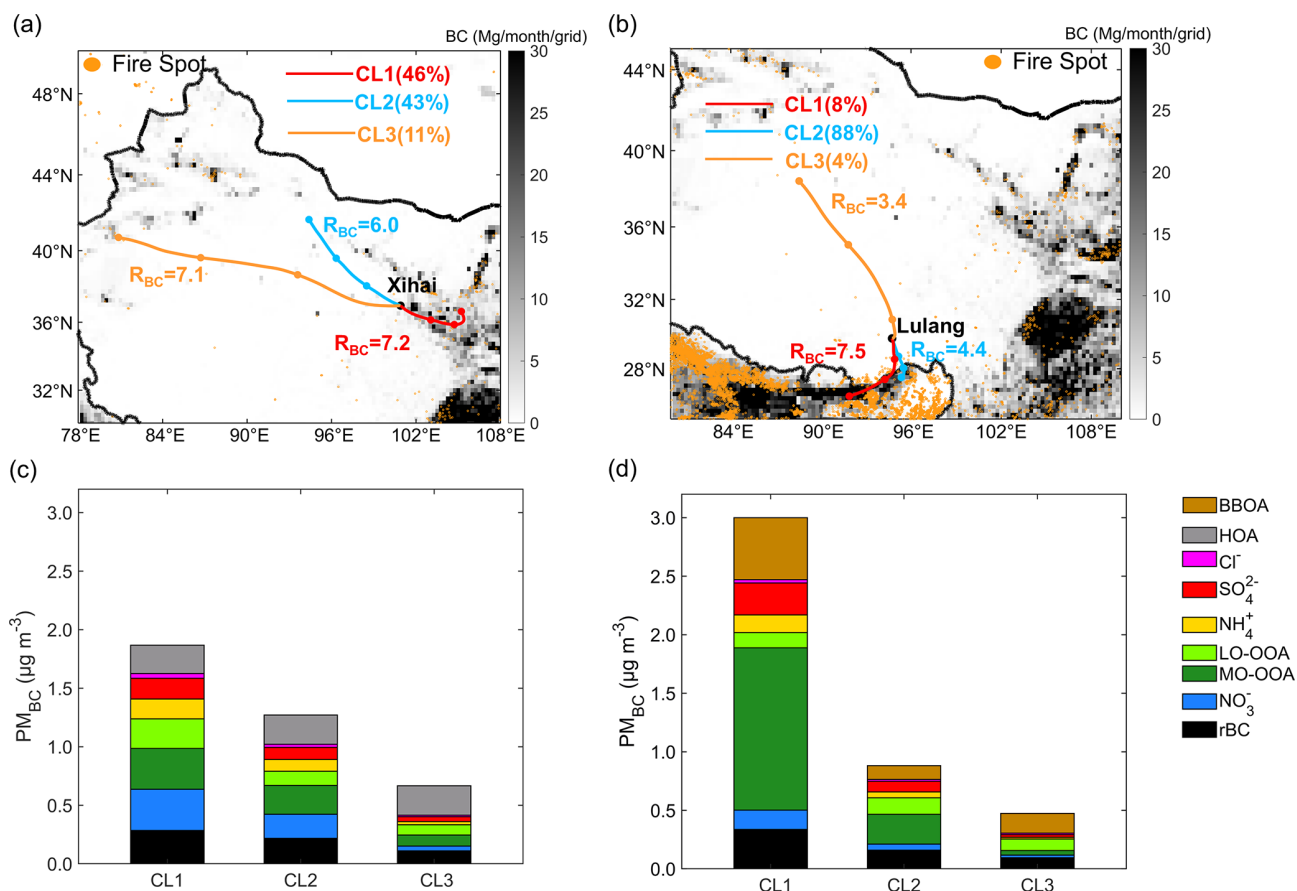


Figure 7. The maps show the backward trajectories in different clusters of (a) Xihai and (b) Lulang. Each circular marker along the trajectories represents a 24 h interval. The background shading represents the anthropogenic BC emission intensity, and the orange spots represent the location of wildfire during the campaign in (a) and (b). The stacked bar plots show the mass concentration of coating components and rBC in (c) Xihai and (d) Lulang.

Table 1. Overview of the BC concentration (mean $\pm 1\sigma$) at different sites of the TP in existing studies. The minimum value and maximum value are shown in parentheses. The measurement results are divided by the black horizontal lines in the table based on different measurement techniques.

Sampling site	Location	Instrument	Sampling period	Altitude (m)	BC concentration ($\mu\text{g m}^{-3}$)	Reference
Lulang	Southeastern TP	SP-AMS	April–May 2021	3300	0.17 \pm 0.17 (0.02–2.22)	This study
Xihai	Northeastern TP	SP-AMS	June 2021	3300	0.24 \pm 0.20 (0.02–1.28)	This study
Qinghai Lake	Northeastern TP	SP2	October 2011	3200	0.36 \pm 0.27 (0.05–1.56)	Wang et al. (2014)
Nann Co	Central TP	SP-AMS	May–June 2015	4730	0.12 \pm 0.085	Wang et al. (2017)
Linzihi	Southeastern TP	AE 16	November 2008–January 2009	3300	0.75 (0.30–1.60)	Cao et al. (2010)
Lulang	Southeastern TP	AE 16	July 2008–August 2009	3300	0.50 \pm 0.52 (0.06–5.37)	Zhao et al. (2017)
Muztagh Ata	Western TP	AE 16	November 2009–September 2010	4500	0.13 \pm 0.06 (0.03–0.33)	Zhu et al. (2016)
Hanle valley	Southern TP	AE 31	August 2009–July 2010	4250	0.077 \pm 0.064 (0.007–0.30)	Babu et al. (2011)
Lulang	Southeastern TP	OC/EC analyzer	July 2008–July 2009	3300	0.52 \pm 0.35	Zhao et al. (2013)
QOMS	Southern TP	OC/EC analyzer	August 2009–July 2010	4276	0.25 \pm 0.22	Cong et al. (2015)
Manora Peak	Southern TP	OC/EC analyzer	February 2005–June 2007	1950	1.0 \pm 0.7 (0.1–2.7)	Ram and Sarin (2009)

To further explore the coupling effect of horizontal and vertical transport on BC in high-altitude regions, both observations and simulations were performed to track the evolution of pollutants in the surrounding area. We chose a typical episode in CL1 in Xihai to conduct model simulations. As illustrated in the zonal profile plots of CO and BC, the high levels of anthropogenic pollutants were uplifted to Xihai (Fig. 8a and b). The updraft flow and the turbulent mixing in the boundary layer carried the anthropogenic emissions from the ground to high altitudes, and then the horizontal easterly winds transported the anthropogenic emissions to the northeast TP. The combination of upward wind and a developing boundary layer (Fig. S8c) allowed the pollutants emitted by the anthropogenic sources near the surface to be carried aloft and transported to the high-altitude TP in the afternoon. This effect can significantly change both the concentration and chemical composition of BC. Compared to the average diurnal variation during observation period, the diurnal variation during episode shows distinctive features (Fig. 8c and d). PM_{BC} concentration increased remarkably from 15:00 (Beijing time) and peaked at 16:00 to 17:00 (Beijing time), with a maximum concentration of $4.0 \mu\text{g m}^{-3}$. Concurrently, NO_3^- and SOA also exhibit a noticeable increase along with the thickening of the BC coating in the afternoon. The NO_3^- , SOA and R_{BC} rose from $0.41 \mu\text{g m}^{-3}$, $0.49 \mu\text{g m}^{-3}$ and 2.8 at 11:00 to $1.06 \mu\text{g m}^{-3}$, $1.31 \mu\text{g m}^{-3}$ and 10.2 at 16:00 (Beijing time, respectively). As Fig. S8a shows, O_3 did not increase significantly after 15:00 (Beijing time) in Xihai, implying that the photochemistry and secondary aerosol formation might not be enhanced. However, the consistent radiative heating of the ground surface during the daytime kept a convective boundary layer (Fig. S8c), facilitating the vertical transport of anthropogenic emissions to higher altitudes and plausibly causing the enhanced air pollution in the afternoon in Xihai. This phenomenon is a good illustration of the vulnerability of remote plateau regions to intense anthropogenic influences, as pollutants can be transported from low-altitude regions to the plateau.

3.4 Impacts of diverse BC coating characteristics on light absorption

The effects of different emission sources on the BC light absorption ability were investigated. Compared to Lulang, the MACs of PM_{BC} were higher in Xihai overall, indicating higher absorption efficiency and potentially stronger radiative forcing in this region. The MACs were all relatively high in three clusters of air masses of Xihai, with the distribution peaking between 12 and $14 \text{ m}^2 \text{ g}^{-1}$ (Fig. 9a), which is numerically comparable to previous studies (Wang et al., 2015). The overall high MAC in Xihai may result from the significant impact of anthropogenic emissions in the northeast TP. The stronger emissions provided abundant precursors of BC coating to improve the coating thickness, and the thick coating enhanced the light absorption capacity of PM_{BC} via the

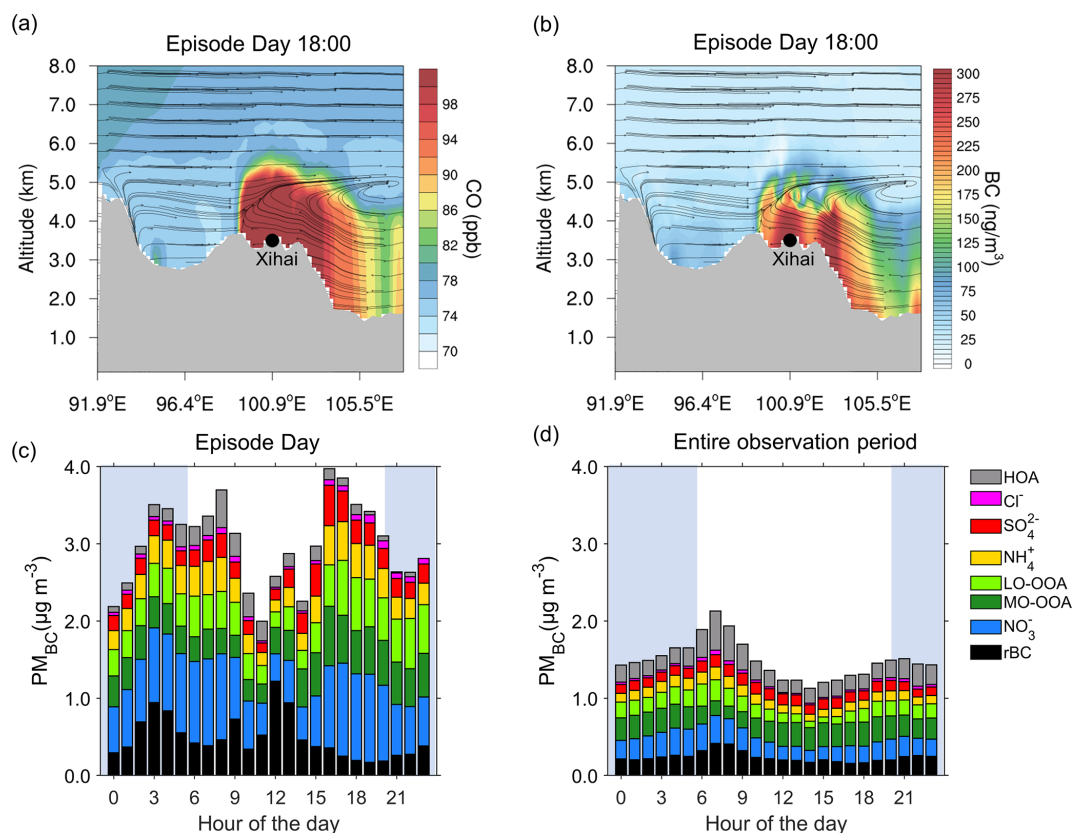


Figure 8. Simulated meridional mean concentration profiles of (a) CO and (b) BC independently during the episode day (19 June 2021). The air circulation is shown as vector arrows, and the terrain height is shown as gray shading in panels (a) and (b). The vertical velocity of wind was amplified by a factor of 3000 for clarity. Panels (c) and (d) show the diurnal variation of BC-containing particle concentration during (c) the episode day and (d) the entire observation period in Xihai. The blue shading represents the nighttime hours during the Xihai campaign in panels (c) and (d). Sunrise in Xihai was at about 06:00 (Beijing time), and sunset was at about 20:30 (Beijing time).

lensing effect, while the MAC was only higher under control of the polluted CL1 air masses in Lulang (Fig. 9b), indicating that the south Asian wildfire plume could significantly strengthen the light absorption ability of BC. The MAC in Lulang was also comparable to previous studies (Wang et al., 2018); the peak of the MAC distribution was $7.6 \text{ m}^2 \text{ g}^{-1}$ at 870 nm ($12.0 \text{ m}^2 \text{ g}^{-1}$ at 550 nm if the absorption Ångström exponent of BC is 1.0). In CL1 air masses of Lulang, the MAC was mainly distributed at the bin between 12 and $14 \text{ m}^2 \text{ g}^{-1}$. That is close to the MAC ($13.1 \text{ m}^2 \text{ g}^{-1}$ at 550 nm) at other TP sites affected by biomass burning plumes (Tan et al., 2021). The BC coating was thick (Fig. 7d) to improve the MAC in CL1 air masses of Lulang influenced by higher BB emissions. These results indicate that strong BB and anthropogenic emissions from the surrounding area could have noticeable impacts on the chemical composition and light absorption ability of BC in the TP, and these impacts were more prevalent in the northeast part of the TP.

4 Conclusions

In this study, we employed the SP-AMS in the laser-only configuration to quantitatively analyze the chemical composition of PM_{BC} at distinct sites, Xihai and Lulang, located in the northeast and southeast regions of the TP. Our findings demonstrate the considerable variability and spatial heterogeneity of BC physical and chemical properties across the TP. Notably, Xihai exhibited higher mass concentrations of rBC and PM_{BC} , with respective mean concentrations of 0.24 and $1.48 \mu\text{g m}^{-3}$, compared to 0.17 and $1.02 \mu\text{g m}^{-3}$ in Lulang. The PM_{BC} in Xihai has a higher aging degree, as indicated by a higher mean R_{BC} of 6.7, in contrast to the mean R_{BC} of 4.5 in Lulang.

The marked differences in chemical composition of PM_{BC} were also observed within the TP region. Due to differences in emission sources, the POA was distinct in Xihai and Lulang. HOA from fossil fuel combustion was one of the main components of PM_{BC} in Xihai as the result of elevated anthropogenic emissions, and there was more BBOA in Lulang, especially when the air masses were from the plains of south

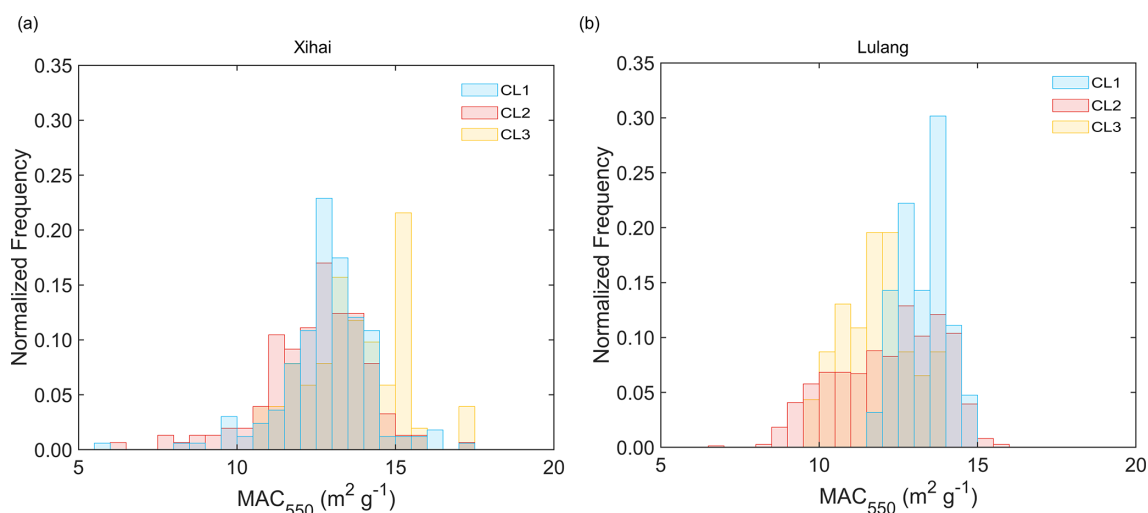


Figure 9. The normalized frequency distribution of the MAC at 550 nm wavelength in different trajectory clusters of (a) Xihai and (b) Lulang.

Asia, affected by frequent wildfire. Besides primary species, the secondary coating components also showed larger differences. The contribution of secondary inorganic aerosols, particularly NO_3^- , was noticeably higher in Xihai because of the strong anthropogenic emission of NO_x as the precursor of NO_3^- . SOA was comparatively higher in areas with less anthropogenic emissions like Lulang. The oxidizing level of SOA was high at both sites of the TP; MO-OOA occupied the largest mass fraction of SOA. We also investigated the variation of PM_{BC} composition with its coating thickness in both sites. An enhancement in NO_3^- fraction was observed on aged BC coating in Xihai. In contrast, the mass contribution of NO_3^- decreased and SOA contribution notably increased during the thickening of PM_{BC} in Lulang.

Backward trajectory analysis and regional chemical transport modeling were then performed to track the impacts of transported anthropogenic and BB emissions on the chemical composition of PM_{BC} in the northeastern and southeastern TP. The effect of anthropogenic emissions was stronger in the northeastern TP when the air masses were brought by updrafts and easterly winds from lower-altitude areas, leading to an increase of NO_3^- and SOA coated on BC. With the development of the boundary layer, strong turbulent mixing promoted the elevation of anthropogenic pollutants. In contrast to Xihai, the thickly coated BC in Lulang was mainly caused by elevation and transportation of biomass burning plumes from south Asia, leading to a significantly higher contribution of MO-OOA and BBOA. The distinct transported emissions caused substantial variations of chemical composition and mixing state of BC, which further changes the light absorption ability of BC in the TP. The MAC of PM_{BC} at both sites was at a high level, showing the strong absorption ability of BC in the TP region, especially in polluted air masses affected by biomass burning emission from south Asia. The overall thicker coating and higher MAC of PM_{BC}

in air masses elevated from lower-altitude regions reveal the impacts of promoted BC aging processes during transportation on the mixing state and light absorption of BC in the TP, which will further influence its radiative effects. Such impacts need to be considered in the evaluation of BC radiative effects for the TP region.

Data availability. The FINN wildfire emission data are available at <https://doi.org/10.5065/XNPA-AF09> (Wiedinmyer and Emons, 2022). The MIX-Asia anthropogenic emission data inventory is available at http://meicmodel.org.cn/?page_id=541&lang=en (MEIC, 2023) and http://meicmodel.org.cn/?page_id=1772&lang=en (MIX, 2021). The boundary layer height (BLH) is acquired from the fifth-generation European Centre for Medium-Range Weather Forecasts (ECMWF) reanalysis data (ERA5; <https://doi.org/10.24381/cds.adbb2d47>, Hersbach et al., 2023). The measurement data covered in the article can be found at <https://doi.org/10.6084/m9.figshare.25399024> (Wang, 2024). Additional data related to this paper may be requested from the authors.

Supplement. The supplement related to this article is available online at: <https://doi.org/10.5194/acp-24-11063-2024-supplement>.

Author contributions. CF, AD, and JiaW conceptualized and supervised this study. JinW, YZ, TL, XC, DG, CZ, LW, XQ and WN conducted the field campaign. JinW and JiaW conducted the data analysis. SL and XH contributed to the model development and simulation. JinW wrote the draft and drew the plots. JiaW, XH and QZ discussed the results. JinW and JiaW reviewed and edited the paper with contributions from all co-authors.

Competing interests. The contact author has declared that none of the authors has any competing interests.

Disclaimer. Publisher's note: Copernicus Publications remains neutral with regard to jurisdictional claims made in the text, published maps, institutional affiliations, or any other geographical representation in this paper. While Copernicus Publications makes every effort to include appropriate place names, the final responsibility lies with the authors.

Acknowledgements. We thank all the co-workers who contributed to the field campaign in Tibetan Plateau. We are grateful for the support of the funders.

Financial support. This work was supported by the second Tibetan Plateau Scientific Expedition and Research (STEP) program (2019QZKK0106) and the National Natural Science Foundation of China (42005082).

Review statement. This paper was edited by Zhibin Wang and reviewed by three anonymous referees.

References

- Akagi, S. K., Yokelson, R. J., Burling, I. R., Meinardi, S., Simpson, I., Blake, D. R., McMeeking, G. R., Sullivan, A., Lee, T., Kreidenweis, S., Urbanski, S., Reardon, J., Griffith, D. W. T., Johnson, T. J., and Weise, D. R.: Measurements of reactive trace gases and variable O₃ formation rates in some South Carolina biomass burning plumes, *Atmos. Chem. Phys.*, 13, 1141–1165, <https://doi.org/10.5194/acp-13-1141-2013>, 2013.
- Babu, S. S., Chaubey, J. P., Moorthy, K. K., Gogoi, M. M., Kompalli, S. K., Sreekanth, V., Bagare, S. P., Bhatt, B. C., Gaur, V. K., Prabhu, T. P., and Singh, N. S.: High altitude (~4520 mamsl) measurements of black carbon aerosols over western trans-Himalayas: Seasonal heterogeneity and source apportionment, *J. Geophys. Res.-Atmos.*, 116, D24201, <https://doi.org/10.1029/2011jd016722>, 2011.
- Bohren, C. F. and Huffman, D. R.: Absorption and scattering of light by small particles, Wiley Science Paperback Series, John Wiley & Sons, New York, NY, USA, 7, <https://doi.org/10.1002/9783527618156>, 1983.
- Bond, T. C. and Bergstrom, R. W.: Light absorption by carbonaceous particles: An investigative review, *Aerosol Sci. Tech.*, 40, 27–67, <https://doi.org/10.1080/02786820500421521>, 2006.
- Bond, T. C., Doherty, S. J., Fahey, D. W., Forster, P. M., Berntsen, T., DeAngelo, B. J., Flanner, M. G., Ghan, S., Karcher, B., Koch, D., Kinne, S., Kondo, Y., Quinn, P. K., Sarofim, M. C., Schultz, M. G., Schulz, M., Venkataraman, C., Zhang, H., Zhang, S., Bellouin, N., Guttikunda, S. K., Hopke, P. K., Jacobson, M. Z., Kaiser, J. W., Klimont, Z., Lohmann, U., Schwarz, J. P., Shindell, D., Storelvmo, T., Warren, S. G., and Zender, C. S.: Bounding the role of black carbon in the climate system: A scientific assessment, *J. Geophys. Res.-Atmos.*, 118, 5380–5552, <https://doi.org/10.1002/jgrd.50171>, 2013.
- Cai, J., Wu, C., Wang, J., Du, W., Zheng, F., Hakala, S., Fan, X., Chu, B., Yao, L., Feng, Z., Liu, Y., Sun, Y., Zheng, J., Yan, C., Bianchi, F., Kulmala, M., Mohr, C., and Daellenbach, K. R.: Influence of organic aerosol molecular composition on particle absorptive properties in autumn Beijing, *Atmos. Chem. Phys.*, 22, 1251–1269, <https://doi.org/10.5194/acp-22-1251-2022>, 2022.
- Canagaratna, M. R., Jayne, J. T., Jimenez, J. L., Allan, J. D., Alfarra, M. R., Zhang, Q., Onasch, T. B., Drewnick, F., Coe, H., Middlebrook, A., Delia, A., Williams, L. R., Trimborn, A. M., Northway, M. J., DeCarlo, P. F., Kolb, C. E., Davidovits, P., and Worsnop, D. R.: Chemical and microphysical characterization of ambient aerosols with the aerodyne aerosol mass spectrometer, *Mass Spectrom. Rev.*, 26, 185–222, <https://doi.org/10.1002/mas.20115>, 2007.
- Canagaratna, M. R., Jimenez, J. L., Kroll, J. H., Chen, Q., Kessler, S. H., Massoli, P., Hildebrandt Ruiz, L., Fortner, E., Williams, L. R., Wilson, K. R., Surratt, J. D., Donahue, N. M., Jayne, J. T., and Worsnop, D. R.: Elemental ratio measurements of organic compounds using aerosol mass spectrometry: characterization, improved calibration, and implications, *Atmos. Chem. Phys.*, 15, 253–272, <https://doi.org/10.5194/acp-15-253-2015>, 2015.
- Cao, J. J., Tie, X. X., Xu, B. Q., Zhao, Z. Z., Zhu, C. S., Li, G. H., and Liu, S. X.: Measuring and modeling black carbon (BC) contamination in the SE Tibetan Plateau, *J. Atmos. Chem.*, 67, 45–60, <https://doi.org/10.1007/s10874-011-9202-5>, 2010.
- Chen, P. F., Kang, S. C., Li, C. L., Zhang, Q. G., Guo, J. M., Tripathee, L., Zhang, Y. A., Li, G., Gul, C., Cong, Z. Y., Wan, X., Niu, H. W., Panday, A. K., Rupakheti, M., and Ji, Z. M.: Carbonaceous aerosol characteristics on the Third Pole: A primary study based on the Atmospheric Pollution and Cryospheric Change (APCC) network, *Environ. Pollut.*, 253, 49–60, <https://doi.org/10.1016/j.envpol.2019.06.112>, 2019.
- Chen, X. Y., Ye, C. X., Wang, Y. Y., Wu, Z. J., Zhu, T., Zhang, F., Ding, X. K., Shi, Z. B., Zheng, Z. H., and Li, W. J.: Quantifying evolution of soot mixing state from trans-boundary transport of biomass burning emissions, *Iscience*, 26, <https://doi.org/10.1016/j.isci.2023.108125>, 2023.
- Cheng, Y., Engling, G., Moosmaller, H., Arnott, W. P., Chen, L. W. A., Wold, C. E., Hao, W. M., and He, K. B.: Light absorption by biomass burning source emissions, *Atmos. Environ.*, 127, 347–354, <https://doi.org/10.1016/j.atmosenv.2015.12.045>, 2016.
- Collier, S., Williams, L. R., Onasch, T. B., Cappa, C. D., Zhang, X. L., Russell, L. M., Chen, C. L., Sanchez, K. J., Worsnop, D. R., and Zhang, Q.: Influence of Emissions and Aqueous Processing on Particles Containing Black Carbon in a Polluted Urban Environment: Insights From a Soot Particle-Aerosol Mass Spectrometer, *J. Geophys. Res.-Atmos.*, 123, 6648–6666, <https://doi.org/10.1002/2017jd027851>, 2018.
- Cong, Z., Kang, S., Kawamura, K., Liu, B., Wan, X., Wang, Z., Gao, S., and Fu, P.: Carbonaceous aerosols on the south edge of the Tibetan Plateau: concentrations, seasonality and sources, *Atmos. Chem. Phys.*, 15, 1573–1584, <https://doi.org/10.5194/acp-15-1573-2015>, 2015.
- Crippa, M., DeCarlo, P. F., Slowik, J. G., Mohr, C., Heringa, M. F., Chirico, R., Poulain, L., Freutel, F., Sciare, J., Cozic, J., Di Marco, C. F., Elsasser, M., Nicolas, J. B., Marchand, N., Abidi, E., Wiedensohler, A., Drewnick, F., Schneider, J., Borrmann, S., Nemitz, E., Zimmermann, R., Jaffrezo, J.-L., Prévôt, A. S. H., and Baltensperger, U.: Wintertime aerosol chemical composition and source apportionment of the organic fraction in the metropolitan area of Paris, *Atmos. Chem. Phys.*, 13, 961–981, <https://doi.org/10.5194/acp-13-961-2013>, 2013.

- Cubison, M. J., Ortega, A. M., Hayes, P. L., Farmer, D. K., Day, D., Lechner, M. J., Brune, W. H., Apel, E., Diskin, G. S., Fisher, J. A., Fuelberg, H. E., Hecobian, A., Knapp, D. J., Mikoviny, T., Riemer, D., Sachse, G. W., Sessions, W., Weber, R. J., Weinheimer, A. J., Wisthaler, A., and Jimenez, J. L.: Effects of aging on organic aerosol from open biomass burning smoke in aircraft and laboratory studies, *Atmos. Chem. Phys.*, 11, 12049–12064, <https://doi.org/10.5194/acp-11-12049-2011>, 2011.
- Cui, S., Huang, D. D., Wu, Y., Wang, J., Shen, F., Xian, J., Zhang, Y., Wang, H., Huang, C., Liao, H., and Ge, X.: Chemical properties, sources and size-resolved hygroscopicity of sub-micron black-carbon-containing aerosols in urban Shanghai, *Atmos. Chem. Phys.*, 22, 8073–8096, <https://doi.org/10.5194/acp-22-8073-2022>, 2022.
- Dall'Osto, M., Harrison, R. M., Coe, H., Williams, P. I., and Allan, J. D.: Real time chemical characterization of local and regional nitrate aerosols, *Atmos. Chem. Phys.*, 9, 3709–3720, <https://doi.org/10.5194/acp-9-3709-2009>, 2009.
- DeCarlo, P. F., Kimmel, J. R., Trimborn, A., Northway, M. J., Jayne, J. T., Aiken, A. C., Gonin, M., Fuhrer, K., Horvath, T., Docherty, K. S., Worsnop, D. R., and Jimenez, J. L.: Field-deployable, high-resolution, time-of-flight aerosol mass spectrometer, *Anal. Chem.*, 78, 8281–8289, <https://doi.org/10.1021/ac061249n>, 2006.
- Docherty, K. S., Jaoui, M., Corse, E., Jimenez, J. L., Offenberg, J. H., Lewandowski, M., and Kleindienst, T. E.: Collection Efficiency of the Aerosol Mass Spectrometer for Chamber-Generated Secondary Organic Aerosols, *Aerosol Sci. Tech.*, 47, 294–309, <https://doi.org/10.1080/02786826.2012.752572>, 2013.
- Drewnick, F., Hings, S. S., DeCarlo, P., Jayne, J. T., Gonin, M., Fuhrer, K., Weimer, S., Jimenez, J. L., Demerjian, K. L., Borrmann, S., and Worsnop, D. R.: A new time-of-flight aerosol mass spectrometer (TOF-AMS) - Instrument description and first field deployment, *Aerosol Sci. Tech.*, 39, 637–658, <https://doi.org/10.1080/02786820500182040>, 2005.
- Duan, A. M. and Wu, G. X.: Role of the Tibetan Plateau thermal forcing in the summer climate patterns over subtropical Asia, *Clim. Dynam.*, 24, 793–807, <https://doi.org/10.1007/s00382-004-0488-8>, 2005.
- Dusek, U., Reischl, G. P., and Hitzenberger, R.: CCN activation of pure and coated carbon black particles, *Environ. Sci. Technol.*, 40, 1223–1230, <https://doi.org/10.1021/es0503478>, 2006.
- Ek, M. B., Mitchell, K. E., Lin, Y., Rogers, E., Grunmann, P., Koren, V., Gayno, G., and Tarpley, J. D.: Implementation of Noah land surface model advances in the National Centers for Environmental Prediction operational mesoscale Eta model, *J. Geophys. Res.-Atmos.*, 108, 8851, <https://doi.org/10.1029/2002JD003296>, 2003.
- Fiddler, M. N., Thompson, C., Pokhrel, R. P., Majluf, F., Canagaratna, M., Fortner, E. C., Daube, C., Roscioli, J. R., Yacovitch, T. I., Herndon, S. C., and Bililign, S.: Emission Factors From Wildfires in the Western US: An Investigation of Burning State, Ground Versus Air, and Diurnal Dependencies During the FIREX-AQ 2019 Campaign, *J. Geophys. Res.-Atmos.*, 129, e2022JD038460, <https://doi.org/10.1029/2022jd038460>, 2024.
- Freitas, S. R., Longo, K. M., Chatfield, R., Latham, D., Silva Dias, M. A. F., Andreae, M. O., Prins, E., Santos, J. C., Gielow, R., and Carvalho Jr., J. A.: Including the sub-grid scale plume rise of vegetation fires in low resolution atmospheric transport models, *Atmos. Chem. Phys.*, 7, 3385–3398, <https://doi.org/10.5194/acp-7-3385-2007>, 2007.
- Fromm, M., Alfred, J., Hoppel, K., Hornstein, J., Bevilacqua, R., Shettle, E., Servranckx, R., Li, Z. Q., and Stocks, B.: Observations of boreal forest fire smoke in the stratosphere by POAM III, SAGE II, and lidar in 1998, *Geophys. Res. Lett.*, 27, 1407–1410, <https://doi.org/10.1029/1999gl011200>, 2000.
- Gao, M., Yang, Y., Liao, H., Zhu, B., Zhang, Y., Liu, Z., Lu, X., Wang, C., Zhou, Q., Wang, Y., Zhang, Q., Carmichael, G. R., and Hu, J.: Reduced light absorption of black carbon (BC) and its influence on BC-boundary-layer interactions during “APEC Blue”, *Atmos. Chem. Phys.*, 21, 11405–11421, <https://doi.org/10.5194/acp-21-11405-2021>, 2021.
- Grell, G. A., Peckham, S. E., Schmitz, R., McKeen, S. A., Frost, G., Skamarock, W. C., and Eder, B.: Fully coupled “online” chemistry within the WRF model, *Atmos. Environ.*, 39, 6957–6975, <https://doi.org/10.1016/j.atmosenv.2005.04.027>, 2005.
- Grell, G. A. and Freitas, S. R.: A scale and aerosol aware stochastic convective parameterization for weather and air quality modeling, *Atmos. Chem. Phys.*, 14, 5233–5250, <https://doi.org/10.5194/acp-14-5233-2014>, 2014.
- Gustafsson, Ö. and Ramanathan, V.: Convergence on climate warming by black carbon aerosols, *P. Natl. Acad. Sci. USA*, 113, 4243–4245, <https://doi.org/10.1073/pnas.1603570113>, 2016.
- Guenther, A., Karl, T., Harley, P., Wiedinmyer, C., Palmer, P. I., and Geron, C.: Estimates of global terrestrial isoprene emissions using MEGAN (Model of Emissions of Gases and Aerosols from Nature), *Atmos. Chem. Phys.*, 6, 3181–3210, <https://doi.org/10.5194/acp-6-3181-2006>, 2006.
- Henning, S., Wex, H., Hennig, T., Kiselev, A., Snider, J. R., Rose, D., Dusek, U., Frank, G. P., Pöschl, U., Kristensson, A., Bilde, M., Tillmann, R., Kiendler-Scharr, A., Mentel, T. F., Walter, S., Schneider, J., Wennrich, C., and Stratmann, F.: Soluble mass, hygroscopic growth, and droplet activation of coated soot particles during LACIS Experiment in November (LExNo), *J. Geophys. Res.-Atmos.*, 115, D11206, <https://doi.org/10.1029/2009jd012626>, 2010.
- Hersbach, H., Bell, B., Berrisford, P., Biavati, G., Horányi, A., Muñoz Sabater, J., Nicolas, J., Peubey, C., Radu, R., Rozum, I., Schepers, D., Simmons, A., Soci, C., Dee, D., and Thépaut, J.-N.: ERA5 hourly data on single levels from 1940 to present, Copernicus Climate Change Service (C3S) Climate Data Store (CDS) [data set], <https://doi.org/10.24381/cds.adbb2d47>, 2023.
- Hong, S. Y., Noh, Y., and Dudhia, J.: A new vertical diffusion package with an explicit treatment of entrainment processes, *Mon. Weather Rev.*, 134, 2318–2341, <https://doi.org/10.1175/mwr3199.1>, 2006.
- Hu, W. W., Hu, M., Hu, W., Jimenez, J. L., Yuan, B., Chen, W. T., Wang, M., Wu, Y. S., Chen, C., Wang, Z. B., Peng, J. F., Zeng, L. M., and Shao, M.: Chemical composition, sources, and aging process of submicron aerosols in Beijing: Contrast between summer and winter, *J. Geophys. Res.-Atmos.*, 121, 1955–1977, <https://doi.org/10.1002/2015jd024020>, 2016.
- Hua, S., Liu, Y. Z., Luo, R., Shao, T. B., and Zhu, Q. Z.: Inconsistent aerosol indirect effects on water clouds and ice clouds over the Tibetan Plateau, *Int. J. Climatol.*, 40, 3832–3848, <https://doi.org/10.1002/joc.6430>, 2020.
- Huang, X., Ding, A., Liu, L., Liu, Q., Ding, K., Niu, X., Nie, W., Xu, Z., Chi, X., Wang, M., Sun, J., Guo, W., and Fu, C.: Effects

- of aerosol–radiation interaction on precipitation during biomass-burning season in East China, *Atmos. Chem. Phys.*, 16, 10063–10082, <https://doi.org/10.5194/acp-16-10063-2016>, 2016.
- Huang, X., Wang, Z., and Ding, A.: Impact of aerosol-PBL interaction on haze pollution: multiyear observational evidences in North China, *Geophys. Res. Lett.*, 45, 8596–8603, 2018.
- Huang, X., Ding, K., Liu, J. Y., Wang, Z. L., Tang, R., Xue, L., Wang, H. K., Zhang, Q., Tan, Z. M., Fu, C. B., Davis, S. J., Andreae, M. O., and Ding, A. J.: Smoke-weather interaction affects extreme wildfires in diverse coastal regions, *Science*, 379, 457–461, <https://doi.org/10.1126/science.add9843>, 2023.
- Kanakidou, M., Seinfeld, J. H., Pandis, S. N., Barnes, I., Dentener, F. J., Facchini, M. C., Van Dingenen, R., Ervens, B., Nenes, A., Nielsen, C. J., Swietlicki, E., Putaud, J. P., Balkanski, Y., Fuzzi, S., Horth, J., Moortgat, G. K., Winterhalter, R., Myhre, C. E. L., Tsigaridis, K., Vignati, E., Stephanou, E. G., and Wilson, J.: Organic aerosol and global climate modelling: a review, *Atmos. Chem. Phys.*, 5, 1053–1123, <https://doi.org/10.5194/acp-5-1053-2005>, 2005.
- Kang, S. C., Xu, Y. W., You, Q. L., Flügel, W. A., Pepin, N., and Yao, T. D.: Review of climate and cryospheric change in the Tibetan Plateau, *Environ. Res. Lett.*, 5, 015101, <https://doi.org/10.1088/1748-9326/5/1/015101>, 2010.
- Kang, S. C., Zhang, Q. G., Qian, Y., Ji, Z. M., Li, C. L., Cong, Z. Y., Zhang, Y. L., Guo, J. M., Du, W. T., Huang, J., You, Q. L., Panday, A. K., Rupakheti, M., Chen, D. L., Gustafsson, Ö., Thiemens, M. H., and Qin, D. H.: Linking atmospheric pollution to cryospheric change in the Third Pole region: current progress and future prospects, *Natl. Sci. Rev.*, 6, 796–809, <https://doi.org/10.1093/nsr/nwz031>, 2019.
- Kim, H., Zhang, Q., and Sun, Y.: Measurement report: Characterization of severe spring haze episodes and influences of long-range transport in the Seoul metropolitan area in March 2019, *Atmos. Chem. Phys.*, 20, 11527–11550, <https://doi.org/10.5194/acp-20-11527-2020>, 2020.
- Kopacz, M., Mauzerall, D. L., Wang, J., Leibensperger, E. M., Henze, D. K., and Singh, K.: Origin and radiative forcing of black carbon transported to the Himalayas and Tibetan Plateau, *Atmos. Chem. Phys.*, 11, 2837–2852, <https://doi.org/10.5194/acp-11-2837-2011>, 2011.
- Labonne, M., Bréon, F. M., and Chevallier, F.: Injection height of biomass burning aerosols as seen from a spaceborne lidar, *Geophys. Res. Lett.*, 34, L11806, <https://doi.org/10.1029/2007gl029311>, 2007.
- Lack, D. A. and Cappa, C. D.: Impact of brown and clear carbon on light absorption enhancement, single scatter albedo and absorption wavelength dependence of black carbon, *Atmos. Chem. Phys.*, 10, 4207–4220, <https://doi.org/10.5194/acp-10-4207-2010>, 2010.
- Lai, S., Qi, X., Huang, X., Lou, S., Chi, X., Chen, L., Liu, C., Liu, Y., Yan, C., Li, M., Liu, T., Nie, W., Kerminen, V.-M., Petäjä, T., Kulmala, M., and Ding, A.: New particle formation induced by anthropogenic–biogenic interactions on the southeastern Tibetan Plateau, *Atmos. Chem. Phys.*, 24, 2535–2553, <https://doi.org/10.5194/acp-24-2535-2024>, 2024.
- Lee, A. K. Y., Chen, C.-L., Liu, J., Price, D. J., Betha, R., Russell, L. M., Zhang, X., and Cappa, C. D.: Formation of secondary organic aerosol coating on black carbon particles near vehicular emissions, *Atmos. Chem. Phys.*, 17, 15055–15067, <https://doi.org/10.5194/acp-17-15055-2017>, 2017.
- Lee, T., Sullivan, A. P., Mack, L., Jimenez, J. L., Kreidenweis, S. M., Onasch, T. B., Worsnop, D. R., Malm, W., Wold, C. E., Hao, W. M., and Collett, J. L.: Chemical Smoke Marker Emissions During Flaming and Smoldering Phases of Laboratory Open Burning of Wildland Fuels, *Aerosol Sci. Tech.*, 44, i–v, <https://doi.org/10.1080/02786826.2010.499884>, 2010.
- Li, M., Liu, H., Geng, G. N., Hong, C. P., Liu, F., Song, Y., Tong, D., Zheng, B., Cui, H. Y., Man, H. Y., Zhang, Q., and He, K. B.: Anthropogenic emission inventories in China: a review, *Natl. Sci. Rev.*, 4, 834–866, <https://doi.org/10.1093/nsr/nwx150>, 2017a.
- Li, M., Zhang, Q., Kurokawa, J.-I., Woo, J.-H., He, K., Lu, Z., Ohara, T., Song, Y., Streets, D. G., Carmichael, G. R., Cheng, Y., Hong, C., Huo, H., Jiang, X., Kang, S., Liu, F., Su, H., and Zheng, B.: MIX: a mosaic Asian anthropogenic emission inventory under the international collaboration framework of the MICS-Asia and HTAP, *Atmos. Chem. Phys.*, 17, 935–963, <https://doi.org/10.5194/acp-17-935-2017>, 2017b.
- Lin, Y. L., Farley, R. D., and Orville, H. D.: Bulk parameterization of the snow field in a cloud model, *J. Clim. Appl. Meteorol.*, 22, 1065–1092, [https://doi.org/10.1175/1520-0450\(1983\)022<1065:BPOTSF>2.0.CO;2](https://doi.org/10.1175/1520-0450(1983)022<1065:BPOTSF>2.0.CO;2), 1983.
- Liu, D. T., Whitehead, J., Alfara, M. R., Reyes-Villegas, E., Spracklen, D. V., Reddington, C. L., Kong, S. F., Williams, P. I., Ting, Y. C., Haslett, S., Taylor, J. W., Flynn, M. J., Morgan, W. T., McFiggans, G., Coe, H., and Allan, J. D.: Black-carbon absorption enhancement in the atmosphere determined by particle mixing state, *Nat. Geosci.*, 10, 184–188, <https://doi.org/10.1038/ngeo2901>, 2017.
- Liu, H., Wang, Q., Xing, L., Zhang, Y., Zhang, T., Ran, W., and Cao, J.: Measurement report: quantifying source contribution of fossil fuels and biomass-burning black carbon aerosol in the southeastern margin of the Tibetan Plateau, *Atmos. Chem. Phys.*, 21, 973–987, <https://doi.org/10.5194/acp-21-973-2021>, 2021.
- Luderer, G., Trentmann, J., Winterrath, T., Textor, C., Herzog, M., Graf, H. F., and Andreae, M. O.: Modeling of biomass smoke injection into the lower stratosphere by a large forest fire (Part II): sensitivity studies, *Atmos. Chem. Phys.*, 6, 5261–5277, <https://doi.org/10.5194/acp-6-5261-2006>, 2006.
- Luo, M., Liu, Y. Z., Zhu, Q. Z., Tang, Y. H., and Alam, K.: Role and Mechanisms of Black Carbon Affecting Water Vapor Transport to Tibet, *Remote Sens.-Basel*, 12, 231, <https://doi.org/10.3390/rs12020231>, 2020.
- Massoli, P., Onasch, T. B., Cappa, C. D., Nuamaan, I., Hakala, J., Hayden, K., Li, S. M., Sueper, D. T., Bates, T. S., Quinn, P. K., Jayne, J. T., and Worsnop, D. R.: Characterization of black carbon-containing particles from soot particle aerosol mass spectrometer measurements on the R/V *Atlantis* during CalNex 2010, *J. Geophys. Res.-Atmos.*, 120, 2575–2593, <https://doi.org/10.1002/2014jd022834>, 2015.
- Mätzler, C.: MATLAB functions for Mie scattering and absorption, version 2, Vol. 8, IAP Res. Rep [code], University of Bern, Bern, Switzerland, 2002.
- Meehl, G. A., Arblaster, J. M., and Collins, W. D.: Effects of black carbon aerosols on the Indian monsoon, *J. Climate*, 21, 2869–2882, <https://doi.org/10.1175/2007jcli1777.1>, 2008.

- MEIC: MEIC-China-Air pollutants, MEIC [data set], http://meicmodel.org.cn/?page_id=541&lang=en (last access: 28 December 2023), 2023.
- Menon, S., Hansen, J., Nazarenko, L., and Luo, Y. F.: Climate effects of black carbon aerosols in China and India, *Science*, 297, 2250–2253, <https://doi.org/10.1126/science.1075159>, 2002.
- MIX: MIX emission inventory, MEIC [data set], http://meicmodel.org.cn/?page_id=1772&lang=en (last access: 28 December 2023), 2021.
- Onasch, T. B., Trimborn, A., Fortner, E. C., Jayne, J. T., Kok, G. L., Williams, L. R., Davidovits, P., and Worsnop, D. R.: Soot Particle Aerosol Mass Spectrometer: Development, Validation, and Initial Application, *Aerosol Sci. Tech.*, 46, 804–817, <https://doi.org/10.1080/02786826.2012.663948>, 2012.
- Pitchford, M., Malm, W., Schichtel, B., Kumar, N., Lowenthal, D., and Hand, J.: Revised algorithm for estimating light extinction from IMPROVE particle speciation data, *J. Air Waste Manage.*, 57, 1326–1336, <https://doi.org/10.3155/1047-3289.57.11.1326>, 2007.
- Ram, K. and Sarin, M. M.: Absorption Coefficient and Site-Specific Mass Absorption Efficiency of Elemental Carbon in Aerosols over Urban, Rural, and High-Altitude Sites in India, *Environ. Sci. Technol.*, 43, 8233–8239, <https://doi.org/10.1021/es9011542>, 2009.
- Ramanathan, V., Chung, C., Kim, D., Bettge, T., Buja, L., Kiehl, J. T., Washington, W. M., Fu, Q., Sikka, D. R., and Wild, M.: Atmospheric brown clouds: Impacts on South Asian climate and hydrological cycle, *P. Natl. Acad. Sci. USA*, 102, 5326–5333, <https://doi.org/10.1073/pnas.0500656102>, 2005.
- Richter, A., Burrows, J. P., Nüss, H., Granier, C., and Niemeier, U.: Increase in tropospheric nitrogen dioxide over China observed from space, *Nature*, 437, 129–132, <https://doi.org/10.1038/nature04092>, 2005.
- Schnaiter, M., Linke, C., Möhler, O., Naumann, K. H., Saathoff, H., Wagner, R., Schurath, U., and Wehner, B.: Absorption amplification of black carbon internally mixed with secondary organic aerosol, *J. Geophys. Res.-Atmos.*, 110, D19204, <https://doi.org/10.1029/2005jd006046>, 2005.
- Sofiev, M., Ermakova, T., and Vankevich, R.: Evaluation of the smoke-injection height from wild-land fires using remote-sensing data, *Atmos. Chem. Phys.*, 12, 1995–2006, <https://doi.org/10.5194/acp-12-1995-2012>, 2012.
- Stein, A. F., Draxler, R. R., Rolph, G. D., Stunder, B. J. B., Cohen, M. D., and Ngan, F.: NOAA'S HYSPLIT ATMOSPHERIC TRANSPORT AND DISPERSION MODELING SYSTEM, *B. Am. Meteorol. Soc.*, 96, 2059–2077, <https://doi.org/10.1175/bams-d-14-00110.1>, 2015.
- Sun, P., Nie, W., Chi, X., Xie, Y., Huang, X., Xu, Z., Qi, X., Xu, Z., Wang, L., Wang, T., Zhang, Q., and Ding, A.: Two years of online measurement of fine particulate nitrate in the western Yangtze River Delta: influences of thermodynamics and N₂O₅ hydrolysis, *Atmos. Chem. Phys.*, 18, 17177–17190, <https://doi.org/10.5194/acp-18-17177-2018>, 2018.
- Sun, P., Nie, W., Wang, T., Chi, X., Huang, X., Xu, Z., Zhu, C., Wang, L., Qi, X., Zhang, Q., and Ding, A.: Impact of air transport and secondary formation on haze pollution in the Yangtze River Delta: In situ online observations in Shanghai and Nanjing, *Atmos. Environ.*, 225, 117350, <https://doi.org/10.1016/j.atmosenv.2020.117350>, 2020.
- Sun, Y. L., Wang, Z. F., Wild, O., Xu, W. Q., Chen, C., Fu, P. Q., Du, W., Zhou, L. B., Zhang, Q., Han, T. T., Wang, Q. Q., Pan, X. L., Zheng, H. T., Li, J., Guo, X. F., Liu, J. G., and Worsnop, D. R.: “APEC Blue”: Secondary Aerosol Reductions from Emission Controls in Beijing, *Sci. Rep.-UK*, 6, 20668, <https://doi.org/10.1038/srep20668>, 2016.
- Tan, T., Hu, M., Du, Z., Zhao, G., Shang, D., Zheng, J., Qin, Y., Li, M., Wu, Y., Zeng, L., Guo, S., and Wu, Z.: Measurement report: Strong light absorption induced by aged biomass burning black carbon over the southeastern Tibetan Plateau in pre-monsoon season, *Atmos. Chem. Phys.*, 21, 8499–8510, <https://doi.org/10.5194/acp-21-8499-2021>, 2021.
- Ulbrich, I. M., Canagaratna, M. R., Zhang, Q., Worsnop, D. R., and Jimenez, J. L.: Interpretation of organic components from Positive Matrix Factorization of aerosol mass spectrometric data, *Atmos. Chem. Phys.*, 9, 2891–2918, <https://doi.org/10.5194/acp-9-2891-2009>, 2009.
- Virkkula, A.: Modeled source apportionment of black carbon particles coated with a light-scattering shell, *Atmos. Meas. Tech.*, 14, 3707–3719, <https://doi.org/10.5194/amt-14-3707-2021>, 2021.
- Wang, J.: data(Impacts of elevated anthropogenic emissions on physicochemical characteristic of BC-containing particles in the Tibet Plateau).rar, figshare [data set], <https://doi.org/10.6084/m9.figshare.25399024>, 2024.
- Wang, J., Ge, X., Chen, Y., Shen, Y., Zhang, Q., Sun, Y., Xu, J., Ge, S., Yu, H., and Chen, M.: Highly time-resolved urban aerosol characteristics during springtime in Yangtze River Delta, China: insights from soot particle aerosol mass spectrometry, *Atmos. Chem. Phys.*, 16, 9109–9127, <https://doi.org/10.5194/acp-16-9109-2016>, 2016.
- Wang, J., Wang, J., Cai, R., Liu, C., Jiang, J., Nie, W., Wang, J., Moteki, N., Zaveri, R. A., Huang, X., Ma, N., Chen, G., Wang, Z., Jin, Y., Cai, J., Zhang, Y., Chi, X., Holanda, B. A., Xing, J., Liu, T., Qi, X., Wang, Q., Pohlker, C., Su, H., Cheng, Y., Wang, S., Hao, J., Andreae, M. O., and Ding, A.: Unified theoretical framework for black carbon mixing state allows greater accuracy of climate effect estimation, *Nat. Commun.*, 14, 2703, <https://doi.org/10.1038/s41467-023-38330-x>, 2023.
- Wang, J. F., Zhang, Q., Chen, M. D., Collier, S., Zhou, S., Ge, X. L., Xu, J. Z., Shi, J. S., Xie, C. H., Hu, J. L., Ge, S., Sun, Y. L., and Coe, H.: First Chemical Characterization of Refractory Black Carbon Aerosols and Associated Coatings over the Tibetan Plateau (4730 m a.s.l), *Environ. Sci. Technol.*, 51, 14072–14082, <https://doi.org/10.1021/acs.est.7b03973>, 2017.
- Wang, Q., Cao, J., Han, Y., Tian, J., Zhu, C., Zhang, Y., Zhang, N., Shen, Z., Ni, H., Zhao, S., and Wu, J.: Sources and physicochemical characteristics of black carbon aerosol from the southeastern Tibetan Plateau: internal mixing enhances light absorption, *Atmos. Chem. Phys.*, 18, 4639–4656, <https://doi.org/10.5194/acp-18-4639-2018>, 2018.
- Wang, Q. Y., Schwarz, J. P., Cao, J. J., Gao, R. S., Fahey, D. W., Hu, T. F., Huang, R. J., Han, Y. M., and Shen, Z. X.: Black carbon aerosol characterization in a remote area of Qinghai-Tibetan Plateau, western China, *Sci. Total Environ.*, 479, 151–158, <https://doi.org/10.1016/j.scitotenv.2014.01.098>, 2014.
- Wang, Q. Y., Huang, R.-J., Cao, J. J., Tie, X. X., Ni, H. Y., Zhou, Y. Q., Han, Y. M., Hu, T. F., Zhu, C. S., Feng, T., Li, N., and Li, J. D.: Black carbon aerosol in winter northeastern Qinghai-Tibetan Plateau, China: the source, mixing state

- and optical property, *Atmos. Chem. Phys.*, 15, 13059–13069, <https://doi.org/10.5194/acp-15-13059-2015>, 2015.
- Wiedinmyer, C. and Emmons, L.: Fire Inventory from NCAR version 2 Fire Emission, Research Data Archive at the National Center for Atmospheric Research, Computational and Information Systems Laboratory [data set], <https://doi.org/10.5065/XNPA-AF09>, 2022.
- Wiedinmyer, C., Quayle, B., Geron, C., Belote, A., McKenzie, D., Zhang, X. Y., O'Neill, S., and Wynne, K. K.: Estimating emissions from fires in North America for air quality modeling, *Atmos. Environ.*, 40, 3419–3432, <https://doi.org/10.1016/j.atmosenv.2006.02.010>, 2006.
- Wiedinmyer, C., Akagi, S. K., Yokelson, R. J., Emmons, L. K., Al-Saadi, J. A., Orlando, J. J., and Soja, A. J.: The Fire INventory from NCAR (FINN): a high resolution global model to estimate the emissions from open burning, *Geosci. Model Dev.*, 4, 625–641, <https://doi.org/10.5194/gmd-4-625-2011>, 2011.
- Wiedinmyer, C., Kimura, Y., McDonald-Buller, E. C., Emmons, L. K., Buchholz, R. R., Tang, W., Seto, K., Joseph, M. B., Barsanti, K. C., Carlton, A. G., and Yokelson, R.: The Fire Inventory from NCAR version 2.5: an updated global fire emissions model for climate and chemistry applications, *Geosci. Model Dev.*, 16, 3873–3891, <https://doi.org/10.5194/gmd-16-3873-2023>, 2023.
- Willis, M. D., Lee, A. K. Y., Onasch, T. B., Fortner, E. C., Williams, L. R., Lambe, A. T., Worsnop, D. R., and Abbatt, J. P. D.: Collection efficiency of the soot-particle aerosol mass spectrometer (SP-AMS) for internally mixed particulate black carbon, *Atmos. Meas. Tech.*, 7, 4507–4516, <https://doi.org/10.5194/amt-7-4507-2014>, 2014.
- Wu, G. X., Liu, Y. M., Wang, T. M., Wan, R. J., Liu, X., Li, W. P., Wang, Z. Z., Zhang, Q., Duan, A. M., and Liang, X. Y.: The influence of mechanical and thermal forcing by the Tibetan Plateau on Asian climate, *J. Hydrometeorol.*, 8, 770–789, <https://doi.org/10.1175/jhm609.1>, 2007.
- Wu, G. X., Duan, A. M., Liu, Y. M., Mao, J. Y., Ren, R. C., Bao, Q., He, B., Liu, B. Q., and Hu, W. T.: Tibetan Plateau climate dynamics: recent research progress and outlook, *Natl. Sci. Rev.*, 2, 100–116, <https://doi.org/10.1093/nsr/nwu045>, 2015.
- Xu, B. Q., Cao, J. J., Hansen, J., Yao, T. D., Joswia, D. R., Wang, N. L., Wu, G. J., Wang, M., Zhao, H. B., Yang, W., Liu, X. Q., and He, J. Q.: Black soot and the survival of Tibetan glaciers, *P. Natl. Acad. Sci. USA*, 106, 22114–22118, <https://doi.org/10.1073/pnas.0910444106>, 2009.
- Xu, J., Zhang, Q., Shi, J., Ge, X., Xie, C., Wang, J., Kang, S., Zhang, R., and Wang, Y.: Chemical characteristics of sub-micron particles at the central Tibetan Plateau: insights from aerosol mass spectrometry, *Atmos. Chem. Phys.*, 18, 427–443, <https://doi.org/10.5194/acp-18-427-2018>, 2018.
- Yang, J. H., Kang, S. C., Chen, D. L., Zhao, L., Ji, Z. M., Duan, K. Q., Deng, H. J., Tripathee, L., Du, W. T., Rai, M., Yan, F. P., Li, Y., and Gillies, R. R.: South Asian black carbon is threatening the water sustainability of the Asian Water Tower, *Nat. Commun.*, 13, 7360, <https://doi.org/10.1038/s41467-022-35128-1>, 2022.
- Yang, K., Wu, H., Qin, J., Lin, C. G., Tang, W. J., and Chen, Y. Y.: Recent climate changes over the Tibetan Plateau and their impacts on energy and water cycle: A review, *Global Planet. Change*, 112, 79–91, <https://doi.org/10.1016/j.gloplacha.2013.12.001>, 2014.
- Yao, T. D., Thompson, L., Mosbrugger, V., Zhang, F., Ma, Y., Luo, T., Xu, B., Yang, X., Joswiak, D. R., Wang, W., Joswiak, M. E., Devkota, L. P., Tayal, S., Jilani, R., and Fayziev, R.: Third Pole Environment (TPE), *Environ. Dev.*, 3, 52–64, <https://doi.org/10.1016/j.envdev.2012.04.002>, 2012a.
- Yao, T. D., Thompson, L., Yang, W., Yu, W. S., Gao, Y., Guo, X. J., Yang, X. X., Duan, K. Q., Zhao, H. B., Xu, B. Q., Pu, J. C., Lu, A. X., Xiang, Y., Kattel, D. B., and Joswiak, D.: Different glacier status with atmospheric circulations in Tibetan Plateau and surroundings, *Nat. Clim. Change*, 2, 663–667, <https://doi.org/10.1038/nclimate1580>, 2012b.
- Yuan, Q., Xu, J. Z., Wang, Y. Y., Zhang, X. H., Pang, Y. E., Liu, L., Bi, L., Kang, S. C., and Li, W. J.: Mixing State and Fractal Dimension of Soot Particles at a Remote Site in the Southeastern Tibetan Plateau, *Environ. Sci. Technol.*, 53, 8227–8234, <https://doi.org/10.1021/acs.est.9b01917>, 2019.
- Zaveri, R. A. and Peters, L. K.: A new lumped structure photochemical mechanism for large-scale applications, *J. Geophys. Res.-Atmos.*, 104, 30387–30415, <https://doi.org/10.1029/1999jd900876>, 1999.
- Zaveri, R. A., Easter, R. C., Fast, J. D., and Peters, L. K.: Model for Simulating Aerosol Interactions and Chemistry (MOSAIC), *J. Geophys. Res.-Atmos.*, 113, D13204, <https://doi.org/10.1029/2007JD008782>, 2008.
- Zhang, M., Zhao, C., Cong, Z., Du, Q., Xu, M., Chen, Y., Chen, M., Li, R., Fu, Y., Zhong, L., Kang, S., Zhao, D., and Yang, Y.: Impact of topography on black carbon transport to the southern Tibetan Plateau during the pre-monsoon season and its climatic implication, *Atmos. Chem. Phys.*, 20, 5923–5943, <https://doi.org/10.5194/acp-20-5923-2020>, 2020.
- Zhang, Q., Worsnop, D. R., Canagaratna, M. R., and Jimenez, J. L.: Hydrocarbon-like and oxygenated organic aerosols in Pittsburgh: insights into sources and processes of organic aerosols, *Atmos. Chem. Phys.*, 5, 3289–3311, <https://doi.org/10.5194/acp-5-3289-2005>, 2005a.
- Zhang, Q., Alfarra, M. R., Worsnop, D. R., Allan, J. D., Coe, H., Canagaratna, M. R., and Jimenez, J. L.: Deconvolution and quantification of hydrocarbon-like and oxygenated organic aerosols based on aerosol mass spectrometry, *Environ. Sci. Technol.*, 39, 4938–4952, <https://doi.org/10.1021/es048568l>, 2005b.
- Zhang, Q., Jimenez, J. L., Canagaratna, M. R., Ulbrich, I. M., Ng, N. L., Worsnop, D. R., and Sun, Y. L.: Understanding atmospheric organic aerosols via factor analysis of aerosol mass spectrometry: a review, *Anal. Bioanal. Chem.*, 401, 3045–3067, 2011.
- Zhang, R., Wang, H., Qian, Y., Rasch, P. J., Easter, R. C., Ma, P.-L., Singh, B., Huang, J., and Fu, Q.: Quantifying sources, transport, deposition, and radiative forcing of black carbon over the Himalayas and Tibetan Plateau, *Atmos. Chem. Phys.*, 15, 6205–6223, <https://doi.org/10.5194/acp-15-6205-2015>, 2015.
- Zhang, X., Xu, J., Kang, S., Liu, Y., and Zhang, Q.: Chemical characterization of long-range transport biomass burning emissions to the Himalayas: insights from high-resolution aerosol mass spectrometry, *Atmos. Chem. Phys.*, 18, 4617–4638, <https://doi.org/10.5194/acp-18-4617-2018>, 2018.
- Zhao, D., Schmitt, S. H., Wang, M., Acir, I.-H., Tillmann, R., Tan, Z., Novelli, A., Fuchs, H., Pullinen, I., Wegener, R., Rohrer, F., Wildt, J., Kiendler-Scharr, A., Wahner, A., and Mentel, T. F.: Effects of NO_x and SO₂ on the secondary organic aerosol formation from photooxidation of α -pinene and limonene, *At-*

- mos. Chem. Phys., 18, 1611–1628, <https://doi.org/10.5194/acp-18-1611-2018>, 2018.
- Zhao, Z. Z., Cao, J. J., Shen, Z. X., Xu, B. Q., Zhu, C. S., Chen, L. W. A., Su, X. L., Liu, S. X., Han, Y. M., Wang, G. H., and Ho, K. F.: Aerosol particles at a high-altitude site on the Southeast Tibetan Plateau, China: Implications for pollution transport from South Asia, *J. Geophys. Res.-Atmos.*, 118, 11360–11375, <https://doi.org/10.1002/jgrd.50599>, 2013.
- Zhao, Z. Z., Wang, Q. Y., Xu, B. Q., Shen, Z. X., Huang, R. J., Zhu, C. S., Su, X. L., Zhao, S. Y., Long, X., Liu, S. X., and Cao, J. J.: Black carbon aerosol and its radiative impact at a high-altitude remote site on the southeastern Tibet Plateau, *J. Geophys. Res.-Atmos.*, 122, 5515–5530, <https://doi.org/10.1002/2016jd026032>, 2017.
- Zheng, G. J., Sedlacek, A. J., Aiken, A. C., Feng, Y., Watson, T. B., Raveh-Rubin, S., Uin, J., Lewis, E. R., and Wang, J.: Long-range transported North American wildfire aerosols observed in marine boundary layer of eastern North Atlantic, *Environ. Int.*, 139, 105680, <https://doi.org/10.1016/j.envint.2020.105680>, 2020.
- Zhou, W., Wang, Q., Zhao, X., Xu, W., Chen, C., Du, W., Zhao, J., Canonaco, F., Prévôt, A. S. H., Fu, P., Wang, Z., Worsnop, D. R., and Sun, Y.: Characterization and source apportionment of organic aerosol at 260 m on a meteorological tower in Beijing, China, *Atmos. Chem. Phys.*, 18, 3951–3968, <https://doi.org/10.5194/acp-18-3951-2018>, 2018.
- Zhu, C. S., Cao, J. J., Xu, B. Q., Huang, R. J., Wang, P., Ho, K. F., Shen, Z. X., Liu, S. X., Han, Y. M., Tie, X. X., Zhao, Z. Z., and Chen, L. W. A.: Black Carbon Aerosols at Mt. Muztagh Ata, a High-Altitude Location in the Western Tibetan Plateau, *Aerosol Air Qual. Res.*, 16, 752–763, <https://doi.org/10.4209/aaqr.2015.04.0255>, 2016.
- Zhu, C. S., Cao, J. J., Hu, T. F., Shen, Z. X., Tie, X. X., Huang, H., Wang, Q. Y., Huang, R. J., Zhao, Z. Z., Mocnik, G., and Hansen, A. D. A.: Spectral dependence of aerosol light absorption at an urban and a remote site over the Tibetan Plateau, *Sci. Total Environ.*, 590, 14–21, <https://doi.org/10.1016/j.scitotenv.2017.03.057>, 2017.